Biofuel Research Journal 43 (2024) 2194-2210

Biofuel Research Journal

Journal homepage: www.biofueljournal.com

Original Research Paper

Advanced computational modelling for biofuel catalyst optimization: enhancing beta zeolite acidity for oleic acid upgrading

Seba AlAreeqi[1], Daniel Bahamon[1], Ismail I.I. Alkhatib[1], Kyriaki Polychronopoulou[2,*], Lourdes F. Vega[1,*]

[1]*Research and Innovation Center on CO_2 and Hydrogen (RICH Center) and Chemical and Petroleum Engineering Department, Khalifa University of Science and Technology, Abu Dhabi, PO Box 127788, UAE.*

[2]*Center for Catalysis and Separations (CeCaS) and Mechanical and Nuclear Engineering Department, Khalifa University of Science and Technology, Abu Dhabi, P.O. Box 127788, UAE.*

HIGHLIGHTS

- Oleic acid upgrading on Beta zeolite of fine−tuned acidity explored by Reactive force field (ReaxFF) simulations.
- The ReaxFF model reproduced an experimental conversion of 50% for the silica-to-aluminium ratio (SAR) of 20.
- SAR=37.4 attained the highest conversion (69.8%) and biofuels yields (>15 wt%) with intermediate coking (8.6 wt%).
- ReaxFF simulations can be employed to study coke yield and thermochemical metrics.
- Screening of metallic co-catalysts favors Cu-doping, having reduced carbon deposition susceptibility relative to V, Mo, W, Co, and Ni.

GRAPHICAL ABSTRACT

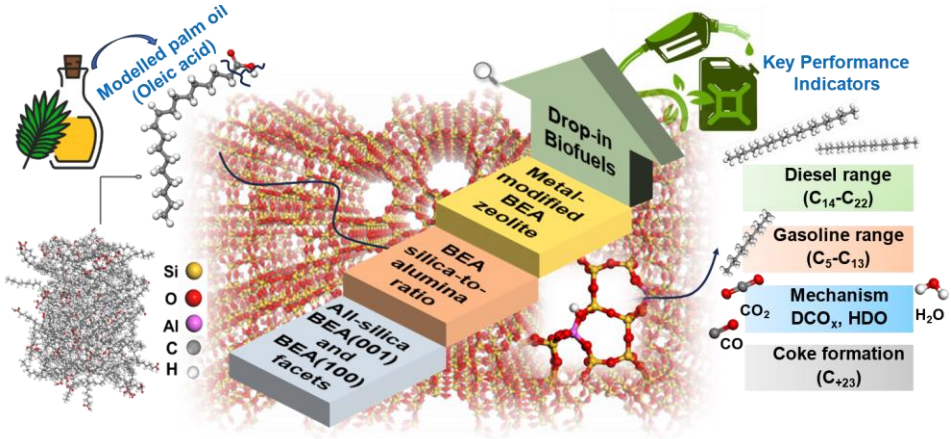

ARTICLE INFO

Article history:
Received 4 May 2024
Received in revised form 30 July 2024
Accepted 1 August 2024
Published 1 September 2024

Keywords:
Oleic acid
Deoxygenation
Zeolite
Reactive force field molecular dynamics simulations
Silica to aluminium ratio
Density functional theory

ABSTRACT

We explore here, through reactive force field (ReaxFF) molecular dynamics simulations, oleic acid upgrading on beta zeolite (BEA) regulated with nine silica-to-aluminium ratios (SARs) to investigate their acid-catalyzed deoxygenation and coking susceptibility. The selected computational descriptors involved conversion, hydrodeoxygenation, and decarboxylation/decarbonylation selectivity, biofuels yield, and coke deposition characteristics. Simulations were validated by 20.3 SAR available experimental data and used for the systematic study. High deoxygenation selectivity was found to be related to the structural sensitivity of BEA(100) on the upgrading mechanism. ReaxFF simulations revealed that altering the Al-substitution could greatly promote biofuel formation. Specifically, SARs towards the mid-region (SAR 47) favored gasoline production, while 31 SAR exploited diesel-like hydrocarbons. An optimum ratio of 37.4 SAR achieved maximum oleic acid conversion (69.8%), with high yields of gasoline and diesel fuels (15.6 and 20.4 wt%, respectively) and moderate coking (8.6 wt%). Density functional theory screening of metallic dopants allowed investigating of their deoxygenation and coke susceptibility, obtaining that Cu-BEA structure favored the optimal carbon and O−moiety adsorption (-3.89 and -1.8 eV, respectively). Furthermore, the economic and environmental analysis showed that Cu-dopped BEA displayed the lowest market price and global warming potential (71 USD/kg and 2.8 kg CO_2-eq/kg).

* Corresponding authors at:
E-mail address: kyriaki.polychrono@ku.ac.ae (Kyriaki Polychronopoulou); lourdes.vega@ku.ac.ae (Lourdes F. Vega)

Please cite this article as: AlAreeqi S., Bahamon D., Alkhatib I.I.I., Polychronopoulou K., Vega L.F. Advanced computational modelling for biofuel catalyst optimization: enhancing beta zeolite acidity for oleic acid upgrading. Biofuel Research Journal 43 (2024) 2194-2210. DOI: 10.18331/BRJ2024.11.3.5.

Contents

Abbreviations

BEA	Beta zeolite
COC	Cellulose-oil composite
CTUh	Comparative toxic units
DCO	Decarbonylation
DCO_2	Decarboxylation
DCO_x	Decarboxylation/decarbonylation
DFT	Density functional theory
DH	Dehydrogenation
E_{ads}	Adsorption energy
GWP	Global warming potential
HCs	Hydrocarbons
HDO	Hydrodeoxygenation
HHV	Higher heating value
LAMMPS	Large-scale Atomic/Molecular Massively Parallel Simulator
LCA	Life cycle assessment
OA	Oleic acid
QM	Quantum mechanics
ReaxFF	Reactive force field
SAC	Single-atom catalyst
SARs	Silica-to-aluminium ratios
SiOC	Siliconoxycarbide
VASP	Vienna Ab-Initio Simulation Packa

1. Introduction

According to the World Energy Outlook (2023), the transportation sector was responsible for about 21.3% of the global energy-related CO_2 emissions in 2022 (Asgarian et al., 2023). Reductions on these transport emissions are envisioned to come by a combination of biofuels (Kargbo et al., 2021) and renewable electricity, depending on the geographical area. In regions such as the United States, Europe, and the People's Republic of China, the use of renewable electricity in transport is estimated to expand eight-fold from 2023-2028, while biofuels remain the primary decarbonization option for the transport sector in the rest of the world, accounting for near 90% of avoided oil demand in 2028. In a recent report on renewables by the International Energy Agency (2024), it is stated that "biofuel demand is set to expand 38 billion L over 2023-2028, a near 30% increase from the last five-year period". The deployment of these technologies would be accelerated by the implementation of planned policies and feedstock diversification, with the United States, Europe, and Japan leading the race. According to the International Energy Agency, active policy discussions in Singapore, Malaysia, Indonesia, India, the United Arab Emirates, Brazil, and the United Kingdom would stimulate an additional 30% increase in biojet fuel demand by 2028.

However, one of the main limitations for the cost-effective scale up of biofuel generation is the availability and diversification of feedstock not competing with other needs (land, water, food). In this sense, second-generation biofuels, also known as advanced biofuels, are an attractive alternative, as they can be manufactured from various types of non-food biomass. Furthermore, given their sulfur-free nature, second-generation biofuels are desirable substitutes for conventional fossil-based fuels, eliminating sulfur emissions to the atmosphere when combusted (Chattopadhyay and Maiti, 2021). Besides, these liquids are upgraded from their highly oxygenated nature to fungible oxygen-free hydrocarbons, resembling the structural features and heating value of petroleum-based fossil fuels (Karatzos et al., 2017; Rambabu et al., 2023). Such properties make them adequate "drop-in" fuels compatible with pre-existing gasoline or diesel fuel engines (Zupko, 2019) without the need to re-design or substitute them.

In terms of biomass feedstocks, palm oil can be regarded as an archetype of an accessible agricultural biomass resource, holding the potential to produce renewable fuels for transportation (Rambabu et al., 2023) and/or as a feedstock for the production of added-value oleochemical products and activated carbon (Chan et al., 2020; Gheewala et al., 2022; Gheewala, 2023). Saturated and monounsaturated fatty acids (i.e., oleic acid and palmitic acid) are the most abundant constitutes of palm oil (Karatzos et al., 2017; Yoosuk et al., 2019).

The deoxygenation reaction mechanisms for palm oil fatty acids to produce biofuels entail three reaction pathways, namely hydrodeoxygenation (HDO), decarboxylation (DCO_2), and decarbonylation (DCO) (Soni et al., 2020). Amidst the three routes reducing the O-content in the produced hydrocarbon biofuel, selective HDO is preferred as it yields water as a by-product (regarded as a green transformation) and also preserves the hydrocarbon functionalities intact, reducing the carbon loss compared to produced CO_2 and CO gases *via* the DCO_2 and DCO routes, respectively (Soni et al., 2020; Kunamalla and Maity, 2023). Thus, the search for heterogenous catalysts that can selectively favor the HDO with respect to the DCO/DCO_2 routes has become a very active area of research.

Several recent experimental studies have focused on the catalytic upgrading of raw vegetable oils or modeled fatty acids to suitable drop-in biofuels. For an in-depth analysis of the HDO, DCO, and DCO_2 deoxygenation pathways of fatty acids upgrading, with an emphasis on the supported catalysts active sites, readers are referred to a comprehensive recent review (Alkhoori et al., 2023). **Table 1** summarizes the catalytic materials, promoters, and conditions of the most relevant experimental work performed on palm oil catalytic upgrading. Oleic acid is widely studied as a representative modelled compound of palm oil feedstock. Yoosuk et al. (2019) targeted the production of diesel fuels from oleic acid over Ni-Mo

Please cite this article as: AlAreeqi S., Bahamon D., Alkhatib I.I.I., Polychronopoulou K., Vega L.F. Advanced computational modelling for biofuel catalyst optimization: enhancing beta zeolite acidity for oleic acid upgrading. Biofuel Research Journal 43 (2024) 2194-2210. DOI: 10.18331/BRJ2024.11.3.5.

Table 1.
Published work in the last five years (2019-2023) for oil fatty acids catalytic upgrading towards biofuels, specifying the catalysts, promoters, silica-to-aluminium ratios (SARs), and upgrading conditions (presence or absence of hydrogen).

Entry	Feedstock	Catalyst Materials	Promoters	Silica-to-aluminium ratio (SAR)	*Ex-situ* Upgrading in the Absence of Hydrogen	H_2 Pressure (bar)	Ref.
1	Oleic acid	Sulfide	Ni-Mo and Co-Mo	-	-	60	Yoosuk et al. (2019)
2	Oleic acid	Al_2O_3/SiO_2	Ni, Co, Ni-Co	-	-	30	Dabbawala et al. (2023)
3	Oleic acid	BEA	La, Co, Fe, Mg, Mn, Zn	25	-	40	Nur Azreena et al. (2021)
4	Crude oil pyrolysis	BEA, HZSM-5	Ni	(BEA) 38, (HZSM-5)30	-	20	Shafaghat et al. (2021)
5	Waste Cooking Oil	SO_4^{2-}/ZnO-BEA	-	-	-	-	Yusuf et al. (2023)
6	Tung oil	SiO_2-Al_2O_3	Co-W	6 & 7	✓	-	Asikin-Mijan et al. (2022)
7	Oleic acid	MgO-Al_2O_3	Ni	-	✓	-	Shi et al. (2023)
8	Oleic acid	BEA Al_2O_3 ZrO_2 HZSM-5 HUSY MCM-41 Activated carbon	Cu-Ni	20	✓	-	Zheng et al. (2020)
9	Oleic acid	BEA	V, Mo, W, Co, Ni, Cu	7, 20.3, 31, 37.4, 47, 68.8, 84.3, 152.6, 255	✓	-	**Present Study**

and Co-Mo catalysts (**Table 1**, *entry 1*). The results revealed that a high H_2 pressure of 60 bar favored high oleic acid conversion and HDO selectivity. Dabbawala et al. (2023) studied the deoxygenation of oleic acid on Ni, Co, and NiCo-doped Al_2O_3/SiO_2 supports utilizing an H_2 pressure of 30 bar (**Table 1**, *entry 2*). Through experiments that were complemented with density functional theory (DFT) calculations, results demonstrated that the DCO_2 and DCO routes were favored on Ni and NiCo, while HDO took place on Co-modified Al_2O_3/SiO_2. Nur Azreena et al. (2021) investigated HDO of oleic acid on BEA zeolite, promoted with various metal dopants (**Table 1**, entry 3), to produce diesel-range fuel. From the studies presented in **Table 1**, it can be concluded that the catalyst active sites play a predominant role in the upgrading mechanism. In most of the works, upgrading of oleic acid was mainly carried out on either zeolites, alumina-silicates, Al_3O_2 supports (Nur Azreena et al., 2021, Dabbawala et al., 2023) and BEA zeolite, referred to in the literature as H-BETA, Hβ, or zeolite-β (Shafaghat et al., 2021, **Table 1**, *entry 4*; Yusuf et al., 2023, **Table 1**, *entry 5*).

In addition to the catalysts, another aspect that is at the frontier of reducing the scalability cost of a palm oil-based biorefinery is sidestepping the use of expensive and hazardous H_2-pressurized vessel environments to drive the HDO (Rashidi et al., 2022; Soltanian et al., 2020). In this regard, Asikin-Mijan et al. (2022) studied oleic acid deoxygenation on a promoted silica-alumina catalyst with Co-W in the absence of H_2 pressure (**Table 1**, *entry 6*). The strategy revolved around utilizing part of oleic acid as a self-H_2 donating candidate, in which dehydrogenation (DH)/cracking reactions would adequately produce the H_2 needed to drive the deoxygenation reaction. Even though the high acidity (i.e., low SAR of 6 and 7) was crucial for the deoxygenation activity, an excess of either acid or base sites was shown to promote the cracking reactions. Such C–C cracking reactions contributed to lowering the yields of the refined hydrocarbon liquid fuels, producing higher fractions of the gaseous products. Shi et al. (2023) showed that MgO-Al_2O_3 promoted with Ni was able to produce green diesel under an H_2-free environment (**Table 1**, *entry 7*). Utilizing oleic acid as a feedstock in the absence of external hydrogen, Zheng et al. (2020) carried out a systematic investigation on BEA, Al_2O_3, ZrO_2, zeolites HZSM-5 and HUSY, activated carbon, and MCM-41 catalytic supports intended for an "*ex-situ*" oleic acid upgrading (see **Table 1**, *entry 8*). Their work tackled the effect of Ni−Cu dopants, the amount of oleic acid injected, and the catalytic temperature.

Gea et al. (2022) revealed that the substitution of tetrahedral Si with trivalent Al atoms plays a critical role in the HDO kinetics of coconut shell pyrolysis oil. Regulating Brønsted acid sites can largely impact their properties and reactivity (Li et al., 2023a). However, to our knowledge, no experimental studies have focused on the effect of tunning the active-sites of BEA zeolite for palm oil upgrading, presenting a significant gap in the use of BEA zeolite for its deoxygenation, which is one of the objectives of the present work (**Table 1**, *entry 9*). Hence, further research is needed regarding fine-tuning the BEA acidity to improve the reaction performance, especially under a hydrogen-free environment. Moreover, the effect of metallic promoters on the catalytic support (see **Table 1**) is scattered in the literature, making it challenging to compare their performance. A systematic assessment of their role in promoting oleic acid deoxygenation would abridge the design of effective functionalized BEA catalysts, which is the objective of this work from a computational perspective (**Table 1**, *entry 9*).

Computational modelling is becoming a standard tool to guide and complement the experimental search for catalytic materials. Among the available tools for this purpose, Reactive Molecular Dynamics simulations can unleash the system reactivity transformations at an atomistic scale without *a-priori* knowledge of the reactant/catalyst reaction pathways and/or possible intermediates. Hence, modelling physical and chemical interactions between atoms using a Reactive force field (ReaxFF) is viewed as a practical and widely applied computational technique for exploring the thermal degradation and stability of complex oxygenated/non-oxygenated carbonaceous-based blends integrated within the energy paradigm of fuel processing and upgrading (Van Duin et al., 2001). Since ReaxFF parametrization is benchmarked on quantum mechanics (QM) interatomic bonding and charges, an accurate representation of bond breakage/formation can be attained at a drastically reduced computational cost. Thus, this technique enables the assessment of the early-stage dynamic evolution for systems in orders-of-magnitude larger than those assessable with QM calculations.

For an in-depth view of the application and ReaxFF-assessed properties of diverse oxygenated-based and hydrocarbon feedstocks, readers are referred to recent reviews (AlAreeqi et al., 2022; Mao et al., 2023), while a summary of the recent ReaxFF studies on biomass and oxygenated molecules, along with their evaluated properties, is presented in **Table 2**.

From the studies listed in **Table 2**, post-processing of the ReaxFF output focused on capturing the reaction pathways and/or number of species. Such properties hinder comparing the ReaxFF findings with experimental studies quantitatively. In this view, the assessment of quantitative ReaxFF quantities, such as biomass conversion and product yields, adds great potential to link the effect of varying critical effects directly to experimental observations. A recent study by Chen et al. (2021) assessed the coke

Please cite this article as: AlAreeqi S., Bahamon D., Alkhatib I.I.I., Polychronopoulou K., Vega L.F. Advanced computational modelling for biofuel catalyst optimization: enhancing beta zeolite acidity for oleic acid upgrading. Biofuel Research Journal 43 (2024) 2194-2210. DOI: 10.18331/BRJ2024.11.3.5.

Table 2.
Advanced ReaxFF computational studies on biomass and oxygenated feedstocks thermochemical conversion and post-processing analysis.

Modelled Biomass Feedstock	Catalytic Material	Qualitative Post-processing			Quantitative Post-processing				Ref.
		Reaction Pathways	Number of Molecules	Radial Distribution Function	Conversion	Yield	O/C Ratio	Selectivity	
Cellulose-oil composite	-	✓	-	-	-	-	-	-	Qu and Li (2023)
Silicone-phenolic hybrid aerogel	-	✓	✓	-	-	-	-	-	Xiao et al. (2023)
Waste cotton	-	✓	-	-	-	-	-	-	Batuer et al. (2021)
Low-rank coal and high-density polyethylene	-	-	-	✓	-	✓	✓	-	Feng et al. (2023)
Polycarbonate	-	✓	✓	-	-	-	-	-	Liu et al. (2021)
Polycyclic aromatic hydrocarbons (PAHs)	Nickel nanocatalyst	✓	✓	✓	✓	✓	-	-	Chen et al. (2021)
Oleic acid	BEA zeolite	✓	✓	✓	✓	✓	✓	✓	**Present Study**

deposition and morphological evolutions of nickel nano-catalysts toward upgrading a lignin-oxygenated feedstock. Not only did the ReaxFF-model quantitatively capture the experimental conversion trend of the lignin pyrolysis, but the reactivity of single- and multi-phenolic/aromatic coke surrogate models were traced to distinguish their collision dynamics, surface-diffusion, and thermal deposition pathways.

Turning to palm oil catalytic deoxygenation, despite the significant improvements in catalytic biomass upgrading, a notable research gap exists in the absence of computational studies of oleic acid upgrading on BEA zeolite coupled with properties that can be linked to experimental outputs. Such molecular-level investigations can provide a comprehensive understanding of the intricate interplay between catalyst properties and deoxygenated fuel production. Specifically, the impact of tuning acidic sites on upgrading conversion, hydrocarbon yield, carbon-range selectivity, and coke deposition tendency remains unclear. Furthermore, elucidating SARs prone to severe coking is essential for developing effective strategies to mitigate catalyst deactivation and improve process efficiency. Abridging these gaps through computational investigations would aid the rational design of zeolite-based catalysts for biomass upgrading applications, ultimately advancing sustainable drop-in biofuel production.

Hence, we present the first computational investigation into oleic acid catalytic upgrading, a key modeled palm oil compound, on BEA zeolite using ReaxFF molecular dynamics simulations to unravel the competitive upgrading/deposition mechanism. First, the methodology on Al-substitutions and silanols-terminations from state-of-art modelling approaches is detailed, along with ReaxFF parameters used in this work benchmarked on QM/experimental work. The effect of the (001) and (100) facets is elucidated, followed by tuning the silica-to-aluminium ratios (SARs) of BEA to exploit their effect on oleic acid conversion, HDO/DCO_x selectivity, and HCs yield, comparing with experimental studies of available SAR. Leveraging the atomistic-level capabilities, the time-evolution upgrading of oleic acid in the microporous local active sites of the structure was mapped out along with the interactions held responsible for coke deposition. Finally, a DFT view into oleic acid O-moieties interactions within BEA vicinity for a wide-range of metallic dopants was explored to abridge their deoxygenation upgrading and carbon-deposition performance.

2. Methodology

2.1. Molecular simulations

The ReaxFF molecular dynamics method, first developed by van Duin et al. (2001), was applied in this work to simulate the reaction mechanism of oleic acid in the zeolite framework. In general, ReaxFF describes the bond formation/breakage through an interatomic potential using a bond-order formalism, thus, allowing studying the chemical reactivity of complex compounds through a sequence of smooth conversion from non-bonded to bonded systems. The total energy of the system is divided into several contributions, as shown in **Equation1** (Kwon et al., 2020):

$$E_{system} = E_{bond} + E_{over} + E_{under} + E_{lp} + E_{val} + E_{tors} + E_{vdWaals} + E_{Coulomb} \quad \text{Eq. 1}$$

where the partial contributions in order of appearance are the bond, over-coordination penalty, under-coordination penalty, lone pair, valence angle energy, torsion angle energy, non-bonded van der Waals, and non-bonded Coulombic energies, respectively. The over-coordination penalty corrects the sum of the total bond order if the atom valence is exceeded according to the valence bond theory, whereas the under-coordination penalty accounts for the π-electron resonance energy contribution. Bonded interactions (i.e., bonds, angles, and torsions) are calculated directly from the interatomic distances using an empirical formula comprising single, double, and triple bond-order contributions. Non-bonded interactions, however, are evaluated using Morse and Coulomb potentials, respectively, between every atomic pair, while the charge polarization within molecules is calculated utilizing an electronegative equalization method approach (Mortier et al., 1986). The bond order is updated after every timestep iteration, allowing the ReaxFF to simulate the bond breakage and formation as the system evolves toward equilibrium.

Simulations were run *via* the ReaxFF package installed in the Large-scale Atomic/Molecular Massively Parallel Simulator (LAMMPS) (Plimpton et al., 2007). The parameters for Si, O, C, H, and Al were obtained from the work of Bai et al. (2012) that were derived from previously developed parameters of van Duin et al. (2003) and Zhang et al. (2005). The canonical ensemble (also known as NVT, i.e., a fixed number of atoms N, volume V, and temperature T) was used in this work. Typically, ReaxFF simulations are run with time steps in the range of 0.1−0.25 fs (Mao et al., 2023). A time step of 0.1 fs integration was used in this work to accurately sample the bond breakage/formation trajectories, as utilized in former ReaxFF work on biofuel combustion (Lele et al., 2021). The temperature was kept constant utilizing the Berendsen thermostat with a 100 fs damping parameter. The selection of the thermostat and damping were based on the settings used in the ReaxFF parametrization work (Bai et al., 2012).

A temperature of 1200 K was employed in the ReaxFF simulations to evaluate the desirable output properties. While experimentally biomass catalytic upgrading is performed at temperatures between 600−773K (Zheng et al., 2020), a common practice of ReaxFF involves employing much higher temperatures than the experimental value to accelerate the reaction kinetics to take place within the ReaxFF simulation time of nanoseconds (Sørensen and Voter, 2000). This approach has proven useful in examining the initial sequence of reactions at the molecular-level, together with providing satisfactory accuracy to experimental studies on various applications such as pyrolysis, combustion, and carbonization (Batuer et al., 2021; Xia et al., 2021; Wei et al., 2023).

To reach the 1200 K at which the production simulations were run, the system was heated up in different steps to avoid instabilities in the simulation energy that may lead to failure in the numerical algorithm (Mao et al., 2023). Hence, the system was first equilibrated for 50 ps at 10 K to set the initial velocities. Then, heated from 10 to 300 K for 50 ps to minimize

Please cite this article as: AlAreeqi S., Bahamon D., Alkhatib I.I.I., Polychronopoulou K., Vega L.F. Advanced computational modelling for biofuel catalyst optimization: enhancing beta zeolite acidity for oleic acid upgrading. Biofuel Research Journal 43 (2024) 2194-2210. DOI: 10.18331/BRJ2024.11.3.5.

the energy of the system and run at 300 K for 100 ps, followed by heating to 700 K for 50 ps, running at 700 K for 100 ps, and heating to 1200 K for 50 ps. The choice of simulation time in the different steps was selected to ensure the relaxation of the system before the new temperature increases. The production run was performed at 1200 K for a time interval of 1000 ps (i.e., 1 ns) to evaluate the desired properties (detailed in *Section 2.1.2*). Moreover, to ensure attaining statistically significant results, the first 800 ps in the production run were used as equilibration, and the last 200 ps were ensemble-averaged to calculate the target properties. Three independent starting configurations were tested to eliminate any bias in the averaged results.

A schematic representation of the ReaxFF workflow is shown in **Figure 1**. The process starts with defining the ReaxFF computational details (i.e., parameter set, time step, damping factor, and temperature) mentioned in the previous paragraphs. The next step involves constructing the simulation model of the oleic acid and varying the zeolite topological and physiochemical properties (explained in detail in *Section 2.1.1*). The results of the ReaxFF simulation are then compared with available experimental data (i.e., yields and selectivity) from the literature. If the ReaxFF matches the experimental findings, the output data is post-processed and analyzed to extract relevant information such as trends in conversion, biofuels yields, upgrading selectivity, microscopic reaction mechanism, and coke characteristics. If the simulation results do not match the experimental data, the process starts by changing some of the input parameters.

2.1.1. Zeolite model development

BEA crystallographic information ($Si_{64}O_{128}$) was obtained from the Structure Commission of the International Zeolite Association. The lattice parameters of the unit cell were first optimized using the Perdew, Burke, and Ernzerhof (PBE) exchange-correlation functional (Perdew et al., 1996), being implemented in the Vienna Ab-Initio Simulation Package (VASP) (Kresse and Furthmüller, 1996). An energy cutoff of 400 eV was used, along with convergence thresholds of 10^{-6} eV and 0.01 eV/Å for the electronic energy and ionic forces, respectively. For the BEA unit cell structural optimization, the obtained lattice parameters were a = b = 12.261 Å and c = 26.016 Å, in excellent agreement with the experimental values (a = b = 12.632 Å and c = 26.186 Å (Corma et al., 2008). The resulting BEA structure was then periodically replicated in all three directions to create a 4×4×2 supercell with sufficient exposed surface and thickness, accounting for the periodicity and confinement effect of the zeolite pore structure.

To obtain structures with different SARs (or Si/Al ratios), Si atoms at the T6 site were replaced with trivalent Al in the all-silica framework, as has been shown in previous DFT screening works to yield the maximum BEA framework stability relative to all possible distinct T-sites (Jones and Iglesia, 2015; Hernandez-Tamargo et al., 2019). To maintain charge neutrality, one proton (H^+) was added to bridging O atoms adjacent to the substituted Al^{4+} at the T6 site, creating the Brønsted acidic sites of microporous aluminosilicates zeolite (Chizallet, 2020), according to the procedure developed by Jones and Iglesia (2015) to yield the lowest deprotonation energy, i.e., highest acidic strength (see **Fig. S1** in the **Supplementary Material** for the exact position of the substituted and added atoms).

As mentioned, the number of Al substitutions was varied to construct models with several SARs. Ratios in the range of high-silica framework (e.g., 255 and 152.6), Al-rich framework (20, 31, and 37.4), and moderate-silica framework (47, 68.8, and 84.3) were considered. In addition, the two-end extremes of all-silica (no aluminum) and SAR = 7 (complete alumination at the T6 site) were simulated, bringing forth a total of 12 distinct structures of BEA zeolite. Considering the Al-substitution stability may also differ depending on the nanopores' crystallographic location (i.e., bulk or external surface), T6 sites near the exposed surface were first replaced, subsequently by Al-substitutions in the bulk nonporous channels, as has been shown that aluminum substitution is thermodynamically most stable (i.e., lowest alumination energy) on the external surface position rather than in bulk (Rey et al., 2017; Chizallet, 2020), provoking the "pore mouth catalysis" concept (Martens et al., 2001).

Figure 2 demonstrates the constructed models for all simulated scenarios of different SAR microporous structures. Eighty-six molecules of oleic acid (density 0.89 g/mL) were added on top of the zeolite surface, as shown in **Figure 2a**. Before examining the role of tunning the acidity, cleavage along the (100) and (001) facets were modeled to study the effect of varying the basal plane orientation on the zeolite behavior (see **Fig. 2b**). In terms of external surface termination, the presence of surface silanols (Si-OH) groups, bridging silica (O-H-O) functionalities, and saturated aluminum substitution (H-O-H) (Rey et al., 2017; Chizallet, 2020) were simulated near the edges to shield the defected framework accounting for the end of growth. These terminations were previously investigated and identified by Wang et al. (2018). Subsequently, the tunned BEA with various SAR were built, yielding a total of 9 distinct frameworks. Shown in **Figure 2c** are the structures for the SAR= 7, 68.8, and 255, while the top and side views of all the 9-tunned SAR BEA microporous frameworks can be found in **Figure S1** (**Supplementary Material**).

An 80 Å vacuum slab was implemented to eliminate any long-range interactions that might come from the z-replicas of the simulation box. The configuration of the zeolite topology and bio-oil multi-molecular feedstock consisted of 9,444 atoms. It should be noted that as the experimental palm oil-to-catalyst ratio typically ranges from 6 to 14 (Taufiqurrahmi et al., 2010), the simulated system, focusing on the molecular-level upgrading near the BEA interface, appoints a feed-to-catalyst ratio of 0.26 due to high

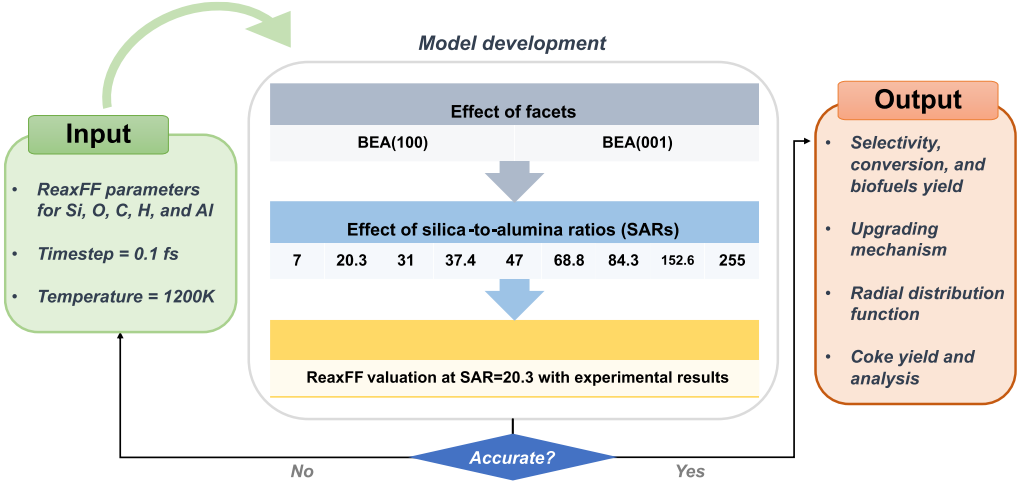

Fig. 1. ReaxFF molecular dynamics workflow used in this work comprising of input specifications, model development, ReaxFF validation with available experimental data, and post-processed simulation output properties.

Please cite this article as: AlAreeqi S., Bahamon D., Alkhatib I.I.I., Polychronopoulou K., Vega L.F. Advanced computational modelling for biofuel catalyst optimization: enhancing beta zeolite acidity for oleic acid upgrading. Biofuel Research Journal 43 (2024) 2194-2210. DOI: 10.18331/BRJ2024.11.3.5.

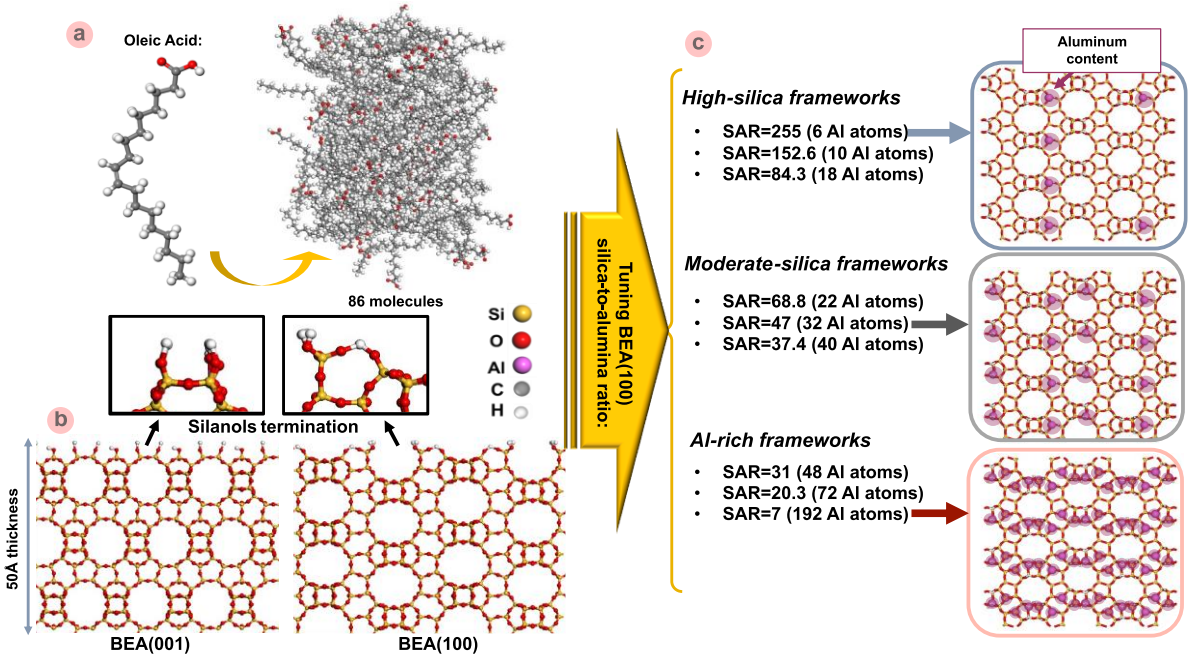

Fig. 2. Simulation model representation of oleic acid, **(a)** multi-component feedstock, **(b)** BEA(001) and BEA(100) with different silanols terminations, and **(c)** design of BEA(100) zeolite structures with tuned SARs from 255 to 7. Note T6-site was chosen for Al-substitution, where SAR = 7 corresponds to fully replaced T6-sites (*Color code: Si: orange, O: red, Al: purple, C: grey, and H: white).*

catalyst concentration with respect to the feed abutting the interface. All atomistic visualization and cluster analysis were produced *via* OVITO (Stukowski, 2010).

2.1.2. Calculated catalytic properties

The catalytic conversion of oleic acid ($X_{oleic\ acid}$) and yield (wt%) were computed as per **Equations 2** and **3**, respectively (Yang et al., 2021):

$$X_{oleic\ acid}(\%) = \frac{n_{oleic\ acid,\ in\ feed} - n_{oleic\ acid,\ in\ product}}{n_{oleic\ acid,\ in\ feed}} \times 100\% \quad \text{Eq. 2}$$

where $n_{oleic\ acid,\ in\ feed}$ is the initial amount (i.e., number of molecules) of oleic acid in the feedstock, while $n_{oleic\ acid,\ in\ product}$ is the non-converted oleic acid amount in the final product mixture.

$$Yield\ (wt\%) = \frac{m_{product}}{m_{oleic\ acid\ feed}} \times 100\% \quad \text{Eq. 3}$$

where $m_{product}$ and $m_{oleic\ acid\ feed}$ denote the masses of the product and oleic acid feedstock, respectively. The light gaseous products' selectivity in the gas phase ($s_{i,gas-phase}$), used to obtain an overview of the upgrading mechanisms of oleic acid on each studied BEA framework with different SAR was computed as per **Equation 4**:

$$s_{i,gas-phase}\ (\%) = \frac{n_{i-gas}}{n_{CO_2} + n_{CO} + n_{H_2O} + n_{H_2}} \times 100\% \quad \text{Eq. 4}$$

where n_{i-gas} represents the number of molecules corresponding to the compound in which the gas selectivity is calculated with respect to (i.e., CO_2, CO, H_2O, or H_2). Moreover, the mass-based hydrocarbons' selectivity within the liquid phase ($s_{i,liquid-phase}$) was also assessed as an important numerical descriptor in the biofuels production analysis from **Equation 5** (Zheng et al., 2020):

$$s_{i,liquid-phase}(wt.\%) = \frac{m_{i-liq}}{m_{total\ liquid}} \times 100\% \quad \text{Eq. 5}$$

where m_{i-liq} is the weight of the liquid compound of interest, while $m_{total\ liquid}$ denote the total weight of liquid phase molecules.

The coking tendency was further characterized by computing the radial distribution function $g(r)$, which is an important index that provides the probability of finding a particle within a three-dimensional distance range of dr. $g(r)$ can be mathematically described as **Equation 6** (Chen et al., 2021):

$$g(r) = \int_0^r 4\pi r^2 \rho dr \quad \text{Eq. 6}$$

where ρ is the local number density at a given distance dr from the reference particle at position 0. The determination of $g(r)$ from the molecular dynamics trajectory data allows a direct comparison of deposited carbonaceous interactions with the BEA framework for each SAR system. All the aforementioned properties were computed after the 800 ps equilibrium heating stage at 1200 K. The analysis of the complex trajectories was performed by examining the bond breakage/formation events of LAMMPS-generated species/bond data over the last 200 ps period.

2.2. Encapsulated M-BEA DFT calculations

While we have established the catalytic influence of the acidic nature of the large-scale BEA framework using ReaxFF, the effect of transition metal dopants is also crucial to the upgrading of oxygenated compounds. For such targeted complex systems, we performed DFT calculations to underpin the effect of BEA doped with transition metals on oleic acid O-functionality cleavage and interactions. Periodic DFT calculations within the generalized gradient approximation (GGA) were performed employing VASP (version 6.2.0) (Kresse and Furthmüller, 1996). The PBE functional (Perdew et al., 1996) with the addition of DFT-D3 correction term (Grimme et al., 2010) was implemented to accurately capture the van der Waals dispersive interactions as extensively applied in previous literature (Bahamon et al., 2021; Bououden et al., 2021; Li et al., 2022). The threshold stopping criterion for electronic convergence was set to 1×10^{-6} eV while forces on each atom were set to be less than 0.01 eV/Å for the ionic loop during geometry optimization (Li et al., 2023b). An energy cutoff of 400 eV was used (Polychronopoulou et al., 2022).

Please cite this article as: AlAreeqi S., Bahamon D., Alkhatib I.I.I., Polychronopoulou K., Vega L.F. Advanced computational modelling for biofuel catalyst optimization: enhancing beta zeolite acidity for oleic acid upgrading. Biofuel Research Journal 43 (2024) 2194-2210. DOI: 10.18331/BRJ2024.11.3.5.

The DFT-optimized BEA unit cell ($Si_{64}O_{128}$) with Al substitution at the T6 site was utilized to construct the BEA co-catalysts modified with transition metals (*i.e.*, M-BEA where M = V, Mo, W, Co, Ni, and Cu). The choice of the metals was made to screen early transition metals (V, Mo, and W) and late transition metals (Co, Ni, and Cu) with varying oxophilicity. These metals have been mostly targeted in biomass HDO reactions considering their abundance, cost-effectiveness, and comparable reactivity to noble metal-based catalysts, making them potential active sites for industrial applications (Yoosuk et al., 2019; Zheng et al., 2020; Asikin-Mijan et al., 2022). The induced charge deficiency resulting from Al substitution in the intra-framework position of BEA was counterbalanced by the transition metal dopants instead of the default hydrogen. Due to the large system taking into consideration the microporous periodic imaging effects, the Brillouin zone sampling was restricted to the Γ-point.

Acetic acid, being representative of the oleic acid carboxylic functional group, was used to truncate the long-range alkyl tail interactions that would significantly slow the computations with minimal effect on O-moiety adsorption and cleavage tendency. This approach has been adopted in previous palm oil DFT work showing reputable results complementing experimental findings (Wongnongwa et al., 2020). The DFT-evaluated key performance indicators were the adsorption energy (E_{ads}), O-M surface separation distance, and C-O bond elongation. The adsorption energy (E_{ads}) was calculated as per **Equation 7**:

$$E_{ads} = E_{M-BEA+adsorbate} - E_{M-BEA} - E_{adsorbate} \quad \text{Eq. 7}$$

where $E_{M-BEA+adsorbate}$ denotes the DFT-calculated energy of the system having M-BEA with the adsorbed acetic acid while E_{M-BEA} and $E_{adsorbate}$ represent the DFT-energy of the separated M-BEA structure and adsorbate in a vacuum, respectively. Combining the adsorption energy with the above bonding characteristics, the C-O bond elongation acts as a suitable reference of facile or unfavorable deoxygenation tendency, while the O-M surface separation distance can serve as a useful index to signify the transition metals poisoning affinity.

3. Results and Discussion

3.1. Effect of (001) and (100) facets on the aggregation and catalytic upgrading of oleic acid on BEA zeolite

We describe here the aggregation behavior of oleic acid on an all-silica BEA catalyst, followed by relating the influence of BEA(001) and BEA(100) facets on the deoxygenation key gaseous products formed, while a quantitative comparison with bio-oil/biomass upgrading experimental studies carried out on BEA zeolite with regulated SARs to tune their acid sites is provided in the subsequent section (*Section 3.2*).

Figure 3 reveals the snapshots of the multi-molecular oleic acid structure evolution at different time intervals of the simulation run, starting from the initial configuration (**Fig. 3 a**). At 300 K, oleic acid aggregates in a micellar configuration due to their tendency to form a liquid phase (**Fig. 3b**). After heating the feedstock to 700 K for 50 ps, the clusteringbehavior of oleic acid changes to disperse to maximize the intermolecular interactions with the BEA zeolite catalyst (**Fig. 3c**). Then, running the simulation at 700 K for 100 ps demonstrates that oleic acid began entering and filling the upper layer microporous structure; however, the long alkyl chains restrain the molecules' relative position to be localized near the entrance (**Fig. 3d**). Interestingly, after heating the system to 1200 K and running the simulations for 1 ns (**Figs. 3 e** and **f**), rapid catalytic upgrading is evident to take place by the cracked hydrocarbons and oxygenated gaseous species depicted.

To quantify the effect of the zeolite support facets on the upgrading mechanism, the number of molecules produced was post-processed from the simulation trajectories at 1200 K, and the gas selectivity of CO_2, CO, H_2O, and H_2 species was calculated, as shown in **Figure 4**. First, the DCO_x, HDO, and DH upgrading mechanisms were evident to take place in our simulation model through the formation of CO_2, CO, H_2O, and H_2 species, respectively, being consistent with the postulated experimental mechanism of DCO_x and HDO for vegetable oils upgrading (Dabbawala et al., 2023), with a greater tendency for DCO_x under *ex-situ* deoxygenation (Zheng et al., 2020). While analogous selectivity towards CO and H_2O molecules formation was found on both (001) and (100) facets, interestingly, almost 2.5-fold CO_2 (21.6%) gas selectivity was achieved on BEA(100) compared to BEA(001) (8.24%), indicating greater tendency of the decarboxylation reaction to take place on this facet.

Alongside the facets pore-opening geometric effects, the silanols chemistry is anticipated to play a key role in probing the catalysis upgrading routes (Medeiros-Costa et al., 2021). In reference to the crystal termination silanols (see **Fig. 2**), the presence of bridge and isolated silanols on the exterior of BEA(100) might contribute to the prevailing DCO_2 mechanism. Conversely, vicinal silanols on BEA(001) did not boost its performance towards oleic acid deoxygenation reactions. Moreover, DH is more dominant on BEA(001), which could manifest in a higher coke-deposition tendency of atomic carbon on the catalyst active sites (Lian et al., 2021). Therefore, BEA(100) exhibits a more favorable net deoxygenation upgrading compared to BEA(001).

3.2. SARs effect on oleic acid conversion and deoxygenation selectivity

Results of oleic acid conversion on the BEA(100) with different SARs are presented in **Figure 5a**. As seen, all modified aluminosilicate scenarios

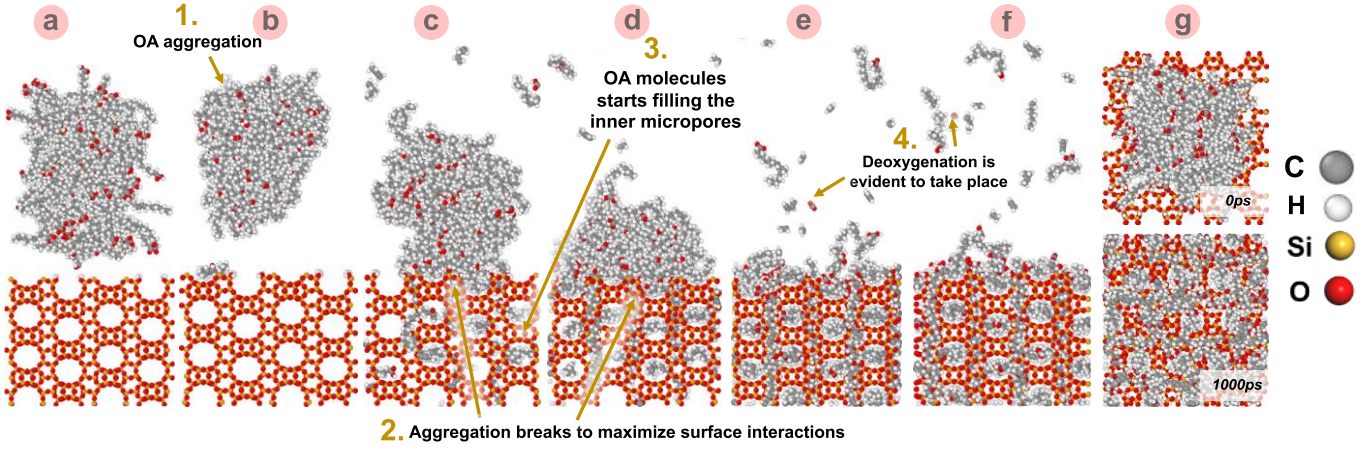

Fig. 3. Dynamic evolution of oleic acid with all-silica BEA(100) structure, **(a)** at the start of the simulation (0 ps), **(b)** 300 K for 100 ps, **(c)** heated to 700 K for 50 ps, **(d)** run at 700 K for 100 ps, **(e)** heated to 1200 K for 50 ps, and **(f)** run at 1200 K for 1000 ps (i.e., 1 ns); **(g)** top views of OA/BEA initial configuration (1st row) and final configuration (2nd row). The dynamic structural distribution of oleic acid (OA) aggregation, adsorption, and reaction at the various time/temperature stages did not vary with respect to (100) and (001) imparted facets..

Please cite this article as: AlAreeqi S., Bahamon D., Alkhatib I.I.I., Polychronopoulou K., Vega L.F. Advanced computational modelling for biofuel catalyst optimization: enhancing beta zeolite acidity for oleic acid upgrading. Biofuel Research Journal 43 (2024) 2194-2210. DOI: 10.18331/BRJ2024.11.3.5.

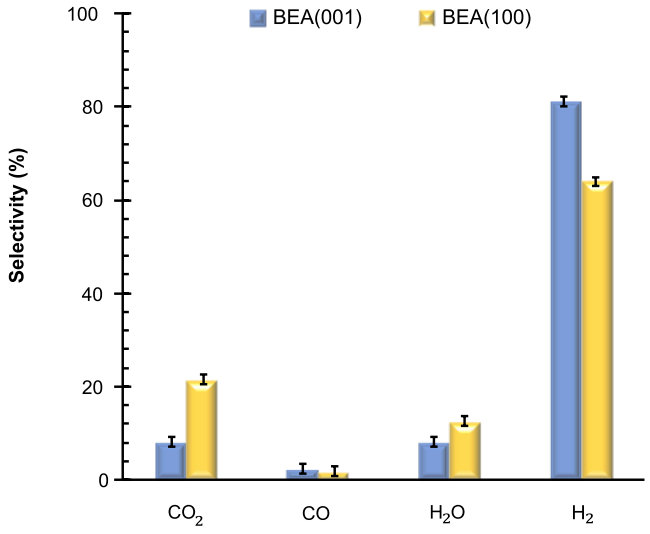

Fig. 4. Calculated gas selectivity (%) of CO_2, CO, H_2O, and H_2 gaseous species produced from oleic acid catalytic upgrading reactions on BEA(001) and BEA(100).

possess an improved conversion of oleic acid ($X_{oleic\ acid}$ = 59.3-69.8%) compared to the all-silica BEA(100) framework ($X_{oleic\ acid}$ = 50%). Yet, distinct variations are evident without a determined clear trend for the SAR. The highest conversion efficiency is attributed to SAR = 37.4 (69.8%), while the lowest is found for SAR = 20.3 (59.3%). Interestingly, fine-tuning BEA(100) SAR to 84.3 provides a further increase in the $X_{oleic\ acid}$ (67.4%), linked to having the optimum BEA acidity at these conditions. This is important as it led to superior catalytic HDO selectivity, as shown in **Figure 5b** and as analyzed next, also contributed to attenuating the undesirable coke-clustering behavior by reducing the acid sites (Li et al., 2023a). This will be particularly underpinned for oleic acid on BEA zeolite in *Section 3.4*.

To reflect on the SAR-mediated effect on the upgrading mechanisms, the degree of H_2O, CO_2, CO, and H_2 production was analyzed in the equilibrated trajectories to quantify the reaction selectivity. Note that due to the trivial fraction of CO molecules produced, the DCO_2 and DCO pathways have been grouped into DCO_x; see **Table S1** in the **Supplementary Material**. The behavior has been classified into three categories: high-SARs, low-SARs, and a mid-transitioning region. In this section, we analyze the gas selectivity performance of the Al-modified BEA zeolites, while the bio-oils interactions and BEA active-sites governing the produced quantities are discussed in-depth in the subsequent section.

Simulation results advocate that the DCO_x reactions were favored to take place compared to HDO, indicative of the high selectivity towards CO_2 and CO (9.2-34.1%) while being lowest for H_2O production (1.7-8.5%). This supports the postulated fatty acids upgrading mechanism in recent experimental studies conducted in the absence of an enriched-H_2 medium or added hydrogen donor (Zheng et al., 2020; Rashidi et al., 2022). Yet, the only comparable DCO_x and HDO selectivity was found at SAR = 7, granted to the abundance of its Brønsted acid sites, recognized to aid oleic acid HDO upgrading (Sudarsanam et al., 2019).

Intriguingly, apart from oleic acid deoxygenation routes, the highest gas selectivity was governed by DH to H_2 gases. A desirable catalyst is one that selectively favors deoxygenation *via* HDO and/or DCO_x compared to rapid DH. As the SAR of BEA microporous frameworks shift from low SARs (i.e., high-aluminium content) to higher ratios (i.e., controlled-aluminium distribution), a gradual reduction in the DH selectivity (−21.8%), accompanied by a steady rise in DCO_x prominence (+24.9%) is witnessed. Thus, as the BEA structure Al-content is lessened from SAR = 7 to 255, oleic acid O-moiety removal *via* DCO_x upgrading was enhanced, while H−cleavage was hindered, thereby less amenable to yield atomic carbon deposition. This gave rise to a higher H/C ratio in the upgraded biofuel and ultimately led to lower CO_2-emissions upon its combustion (Hoffert et al., 1998; Lian et al., 2021). Exploring scaling relations correlating the BEA zeolite SAR (i.e., 20.3-255) to the DCO_x and DH selectivity, linear trends were found useful to guide the prediction of BEA zeolite performance concerning two fundamental reaction routes (**Fig. S2** in the **Supplementary Material**).

3.3. Effect of BEA SARs on biofuels production

To further explore the biofuel hydrocarbon-range products distribution, we calculated the yields of organic gases (C_2-C_4), gasoline (C_5-C_9), diesel (C_{10}-C_{39}), and coke C_{23+} carbonaceous species formed with varying the SAR of BEA zeolite, and results are depicted in **Figure 6**. The production of diesel-range biofuel was found to be the largest across all SARs of BEA(100) catalyst, except for SAR = 84.3, which not only portrayed the highest yield of heavy coke constituents (C_{23+}) but also gave rise to the formation of undesirable short-chain fragmented organic gaseous species. Contemplating the distinct performances, gasoline biofuel production was favored at SARs = 37.4 and 47 (≥15%), while found to be lowest in the highly acidic BEA framework of SAR = 20.3 (7.2%).

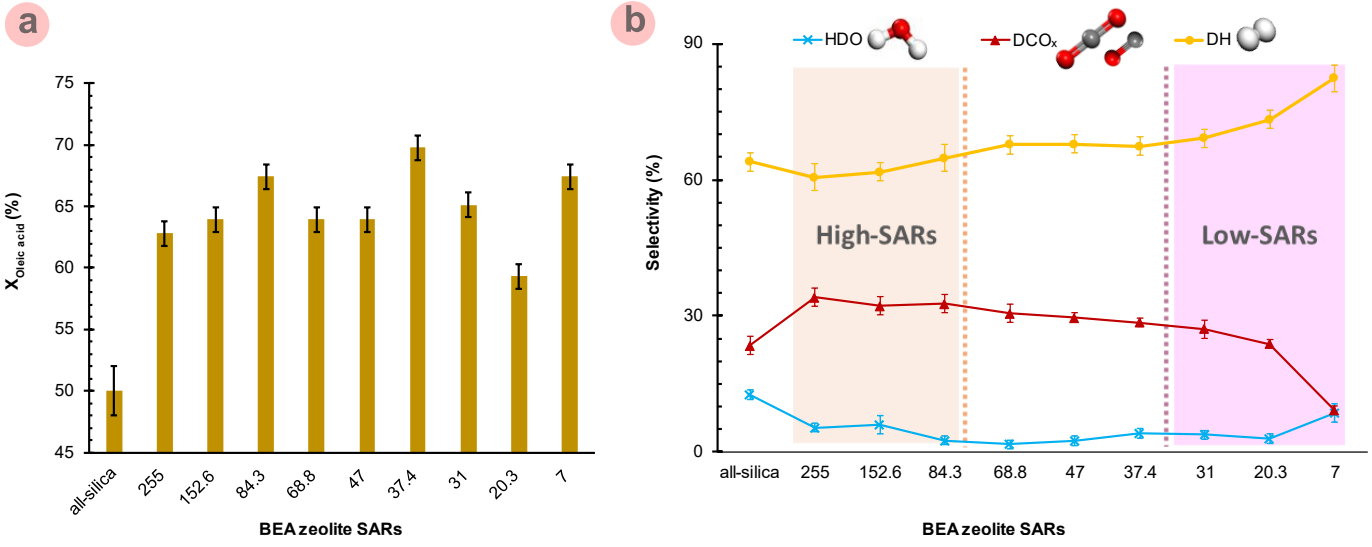

Fig. 5. (a) Oleic acid conversion $X_{oleic\ acid}$ (%) and **(b)** calculated gas selectivity (%) of HDO, $DCO_{x\ (x=1\ and\ 2)}$, DH at various BEA(100) silica-to-aluminium ratios (SARs). The light orange region indicates high-silica ratios, while the purple region indicates the high-aluminium BEA frameworks. Region not shaded holds SARs transitioning between high/low systems

Please cite this article as: AlAreeqi S., Bahamon D., Alkhatib I.I.I., Polychronopoulou K., Vega L.F. Advanced computational modelling for biofuel catalyst optimization: enhancing beta zeolite acidity for oleic acid upgrading. Biofuel Research Journal 43 (2024) 2194-2210. DOI: 10.18331/BRJ2024.11.3.5.

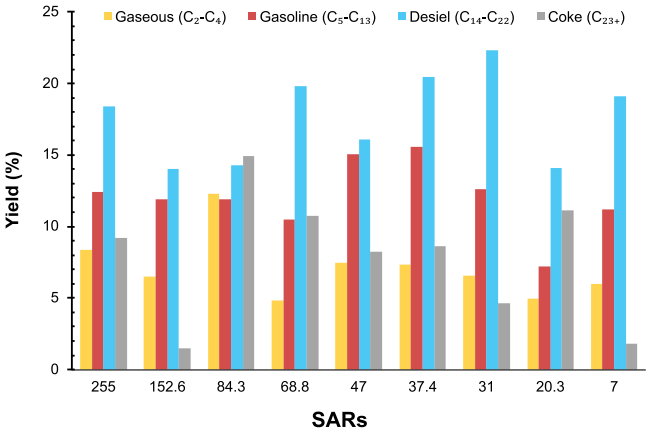

Fig. 6. Yields (wt%) of gaseous (C_2-C_4), gasoline (C_5-C_{13}), diesel (C_{14}-C_{22}), and coke C_{23+} species as a function of BEA(100) SARs (*Color code: yellow stands for gaseous; red for gasoline; blue for diesel; and grey for coke*).

Compared to the diesel biofuel range, SARs 31, 37.4, and 68.8 unveiled an effective tendency to preserve the diesel long-range hydrocarbons intact (≥20%), together with moderate to low generation of coke residues of 4.6% and 8.6% for SARs 31 and 37.4, respectively. Thus, the synthetic control and fine-tuning of the Al distribution in high-silica BEA zeolite is a decisive factor in their high catalytic activity and performance. Our ReaxFF simulation results indicate that a shift to diesel or gasoline production, counterbalanced by averting coke fragments, can be provoked by adjusting the Al substitutional sites. Note that the formation of CH_4 was insignificant (± 1 molecule) across all SAR models. On the contrary, ethylene (C_2H_4) was found to be the predominant gaseous hydrocarbon organic compound (see **Fig. S3c** in the **Supplementary Material**), postulated to form *via* the cleavage of the unsaturated C=C bond within the oleic acid compound. In terms of the largest segment of C-products within the diesel and gasoline biofuels, C_{17} and C_{11} production were most favored (see **Figs. S3a** and **b** in the **Supplementary Material**), respectively, being consistent with the rapid DCO_2 (producing C_{17}).

Table 3 provides a comparison between the results obtained on oleic acid upgrading in this work with available experimental findings on different BEA SARs, conditions, and microporous structures. Considering the environment effect (40 bar of H_2 pressure) in the work of Nur Azreena et al. (2021), the conversion and hydrocarbon yields were significantly boosted, benefiting from the excess hydrogen used to drive the deoxygenation reaction (**Table 3**, *entry 1*). The experimental work performed under H_2-free oleic acid upgrading on BEA with SAR = 20 validates the ReaxFF simulations performed, having comparative conversion and hydrocarbon yields (**Table 3**, *entries 2 and 3*). Nonetheless, we show that tuning the BEA SAR to 37.4 provides higher conversion (70%) and HCs yields (43%) compared to the obtained conversion (59%) and HCs yields (21%) at SAR =20, both evaluated under H_2-free oleic acid upgrading (see **Table 3**, *entries 3 and 4*).

Likewise, in relation to metal-free MCM-41 material, BEA with SAR = 37.4 can efficiently catalyze oleic acid deoxygenation. Higher conversion (from 49 to 70%) and HCs yields (from 39 to 43%) were achieved using the fine-tunned BEA microporous structure instead of MCM-41 (see **Table 3**, *entries 4* and *5*).

However, despite the reported performance of the microporous materials in **Table 3**, catalyst deactivation, dominated by coke deposition, is not often examined. This hampers the comparison of our results with experimental findings. To this extent, in *Section 3.4*, the ReaxFF computational tool is utilized to systematically explore the BEA catalyst coking yields and characteristics (see *Section 3.4*).

Considering additional output properties, **Figure 7** compares the ReaxFF simulation results of this work with the experimental data reported by Zheng et al. (2020) on BEA with SAR = 20. The $X_{oleic\ acid}$ predicted by the ReaxFF model agrees with the experimental value within a 9% difference. Moreover, comparing the experimental selectivity of C_{15}, C_{16}, C_{17}, and C_{18} products with the ReaxFF model, a close correlation is found with the experimental findings. The simulations also perfectly match the HCs yield and HDO/DCO_x of those experimentally determined on BEA of SAR = 20. These findings validate the statistical significance of the ReaxFF-model and simulation approach taken herein, providing confidence in the predictive results in other conditions for which no experimental data is available.

It is worth emphasizing again that a common practice of ReaxFF simulations necessitates elevating the reaction temperature to accelerate the bond breakage/formation events to occur within the simulation timeframe (i.e., nanoseconds) compared to the long experimental time range (i.e., seconds). Wei et al. (2023) established a quantitative agreement of the main gaseous products from cellulose co-gasification with polyethylene between the ReaxFF simulations (1500-1800 K) and experiment (923-1073 K), utilizing a 1.6-fold increased temperature range in the ReaxFF study. A similar approach is made by comparing other ReaxFF simulations in literature to those obtained via experiments (Feng et al., 2023; Pang et al., 2023), proving the versatility and reliability of the C/H/O parameter sets to describe the products evolution.

Once the predictive power of the ReaxFF simulations has been validated by experimental work at SAR=20, our results offer insights into oleic acid upgrading to drop-in carbon-range fuels by tuning the SARs at the atomic level. Thus, we proceed in the subsequent sections to investigate the predominant bio-oil/zeolite interactions held accountable for the enhanced performance, followed by characterizing the coke formation clustering behavior within the BEA microporous channels.

3.4. Initial hydrogenation mechanism on BEA(100) and carbonaceous deposits

The mechanism behind oleic acid upgrading is explored here to provide a deeper understanding of the BEA active-sites role and facilitate the analysis of the carbonaceous deposits. To dissect the molecular-level interactions governing oleic acid behavior with the BEA surface, simulations were conducted using two oleic acid molecules. Attempting to

Table 3.
Comparison of the experimental studies on oleic upgrading with BEA with the ReaxFF results of this study. The work of Zheng et al. (2020) on MCM-41 and doped MCM-41 is added for comparative purposes on the effect of doping on the same catalysts (See the text for details).

Entry	Feedstock	Catalyst	T (K)	H_2 Pressure (bar)	Residence Time (h)	Conversion (%)	Hydrocarbons Yield (%)	Ref.
1	Oleic acid	BEA = 25	623	40	2	99	70	Nur Azreena et al. (2021)
2		BEA = 20	773	-	.	50	23	Zheng et al. (2020)
3		BEA = 20	1200*	-	.	59	21	**Present Study**
4		BEA = 37.4		-	-	70	43	
5		MCM-41	773	-	.	49	39	Zheng et al. (2020)
6		Cu-Ni/ MCM-41	773	-	-	100	86	

* See the methodology regarding the use of this high temperature for the ReaxFF simulations.

Please cite this article as: AlAreeqi S., Bahamon D., Alkhatib I.I.I., Polychronopoulou K., Vega L.F. Advanced computational modelling for biofuel catalyst optimization: enhancing beta zeolite acidity for oleic acid upgrading. Biofuel Research Journal 43 (2024) 2194-2210. DOI: 10.18331/BRJ2024.11.3.5.

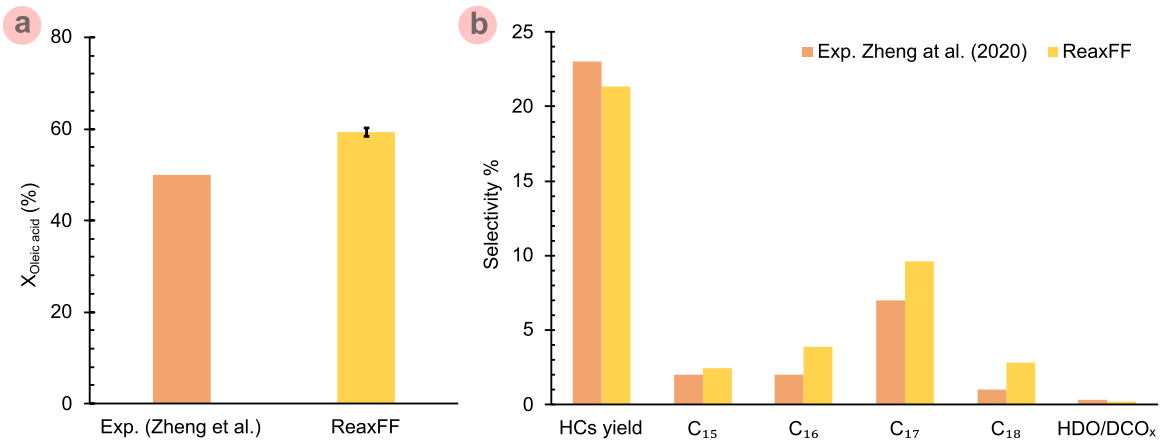

Fig. 7. Comparison between the **(a)** oleic acid conversion, $X_{oleic\ acid}$ (%), and **(b)** hydrocarbon's selectivity and yields of this work's ReaxFF simulation results with Zheng et al. (2020)`s experimental work on oleic acid *ex-situ* catalytic upgrading on BEA zeolite (SAR = 20) [T = 773 and 1200 K for the experiments and ReaxFF simulation, respectively].

breakdown the dynamics, the representative trajectories depicted in **Figure 8a** can be elaborated into four key aspects: initial adsorption, activated H-abstraction of the O-moiety carboxylic group, diffusion, and CO_2 generation. The first step is oleic acid adsorption on the external surface of the open-pore mouth BEA catalyst. Interestingly, a crucial outermost site for the DH of oleic acid is shown to be the bridging silanols (Si-O-H-O-Si), where the weakly H-bonded silanol gains H atom from the carboxylic acid, as illustrated in **Figure 8c**. This serves as the initial catalytic activation step for subsequently cleaving the O-moiety.

Concomitant to surface DH, oleic acid is observed to diffuse through the multi-layer porous structure, where the decarboxylation upgrading reaction (i.e., -CO_2 cleavage) occurs near the protonated acid site (see **Figs. 8a** and **c**). Further interpreting the trajectories, the acidic sites show strong repulsive forces with O-moiety, prevailing CO_2 molecule cleavage to unprotonated pores, while the alkyl tail remains captive within the internal porous structure due to the long-range attractive forces restricting its movement. These structural characteristics provide an understanding of the pathways, revealing the role of initial DH (on the exterior surface) progressed by CO_2 generation (within the second layer). This mechanism, revealed in **Figures 8a** and **c**, was immutably captured for the myriad SARs systems, supporting the conclusion that increasing the acidic sites quantity (beyond the second layer) does not alter the initial deoxygenation upgrading mechanism.

The molecular-level snapshots were also able to uncover that SAR = 152.4, 84.3, and 31 lead to secondary cleavage reactions of unstable long-chain alkyls being decomposed into C_3H_6 and C_2H_2 stacks (**Fig. 8b**). For other systems of high gaseous yields, such as SAR = 255 and 47 (see **Fig. 7**), it is expected that these cracking reactions are induced *via* lateral oleic acid interactions that were not captured with this simplified system comprised of two oleic acid molecules. Nonetheless, we note that with multi-component oleic acid feedstock, extensive DH (see **Fig. 5b**) takes place, satiating the depicted initial cleavage of two oleic acid molecules.

While simulating two oleic acid molecules aids in capturing the initial upgrading mechanism, agglomeration and oligomerization of the oleic acid feedstock would form carbonaceous deposits influenced by the interactions of the straight chain alkyl tails within the porous BEA structure. This bottleneck deactivation lowering the yield of biofuels is explored next. Considering that coke and produced liquid HCs are entangled within the BEA channels, post-processing the intermolecular structural order/strength can provide valuable insights into the carbon functionality most susceptible to deposition.

Plotted in **Figure 9** is the radial distribution function, $g(r)$, descriptive of the structural degree of local order and interaction intensity of oleic acid/BEA zeolite $C_{carbonyl}$–$O_{BEA\text{-}zeolite}$. The $C_{carbonyl}$ of oleic acid appears at 2.7Å from the framework $O_{BEA\text{-}zeolite}$, being the only carbon-moiety in oleic acid that is holding strong bonding interactions with the BEA active-sites. The second peak at 4.7 Å of relatively higher intensity indicates the presence of a long-range disordered amorphous phase, which imparts the absence of crystalline arrangement of the carbonaceous deposits (Chen et al., 2021). In comparison, $C_{carbonyl}$–$O_{BEA\text{-}zeolite}$ peak intensity weakens in the order of 7 > 255 > 37.4 > 84.3 > 31 ≈ 20.3 > 47 > 68.8 for the SARs systems. Interestingly, the anomaly findings impart varying coke susceptibility as the SAR is varied.

Figure 10 shows the C_{23+} coke deposition yield, H/C ratio, O/C ratio, and higher heating value (HHV) with varying BEA zeolite SARs. In terms of quantity, all-silica dictates the lowest coke content (**Fig. 10a**). This is anticipated due to the absence of acid sites that favor coke formation. Moreover, only the oxygenated coke was spotted within this framework, consistent with the well-documented low deoxygenation activity of all-silica mesoporous structure (Grosso-Giordano et al., 2016; Sudarsanam et al., 2019).

Minimal coke having no oxygenated moieties was found to take place on SARs = 31 and 152.6, indicative not only of a high deoxygenation ability but high resistance to oligomerization and condensation reactions. In contrast, SARs = 84.3 and 68.8 showed the highest yield of coke formation, comprising both oxygenated and non-oxygenated constituents. SAR = 20.3 resulted in hydrocarbon-coking, mainly predicted to form due to the oligomerization of deoxygenated oleic acid *via* DCO_2, as the deoxygenated C_{14} chains oligomerize into C_{28} molecules that were detected to intensely appear in BEA SAR = 20.3 coke composition (**Fig. S4** in the **Supplementary Material**). This SAR of BEA was also found to provide high deoxygenation tendencies, yet high coking rates in the work of Zheng et al. (2020).

Regarding the H/C and O/C ratios (see **Fig. 10b**), coke precursor structures of higher volatility (i.e., higher H/C and O/C ratios) are more favorable, as it aids their facile removal *via* combustion into gas phases in the regeneration stage (Ochoa et al., 2020). Nearly comparable H/C ratios exhibiting similar molecular weight characteristics were identified (H/C≈1.87-1.91), while a relatively condensed coking behavior was observed at SAR = 31 and SAR = 7 (H/C≈1.80-1.83). The trivial low O/C indicates that the nature of oxygenated coke mainly features carboxylic moieties. These precursors of oxygenated content attached to long carbon-chain tails yield coke structures of low O/C, formed *via* condensation, isomerization, and polymerization reactions of oleic acid intermediates.

Regarding coke elemental analysis, the HHV can be assessed as a useful index of the coke heat released upon undergoing combustion. While all-silica exhibits an HHV of 43 MJ/Kg, modified BEA(100) systems reveal raised HHV values of 46.2-49.3 MJ/Kg depending on the employed SAR (see **Fig. 10c**). This increase in coke combustion exothermic nature minimizes the heat requirements in the catalyst regeneration step (Ochoa et al., 2020). Note that HHV displays an inversely proportional profile resembling that of the O/C ratio as interpreted from Dulong's formula utilized in this work (see **Supplementary Material**) and in correspondence to experimental work (Ochoa et al., 2018).

Please cite this article as: AlAreeqi S., Bahamon D., Alkhatib I.I.I., Polychronopoulou K., Vega L.F. Advanced computational modelling for biofuel catalyst optimization: enhancing beta zeolite acidity for oleic acid upgrading. Biofuel Research Journal 43 (2024) 2194-2210. DOI: 10.18331/BRJ2024.11.3.5.

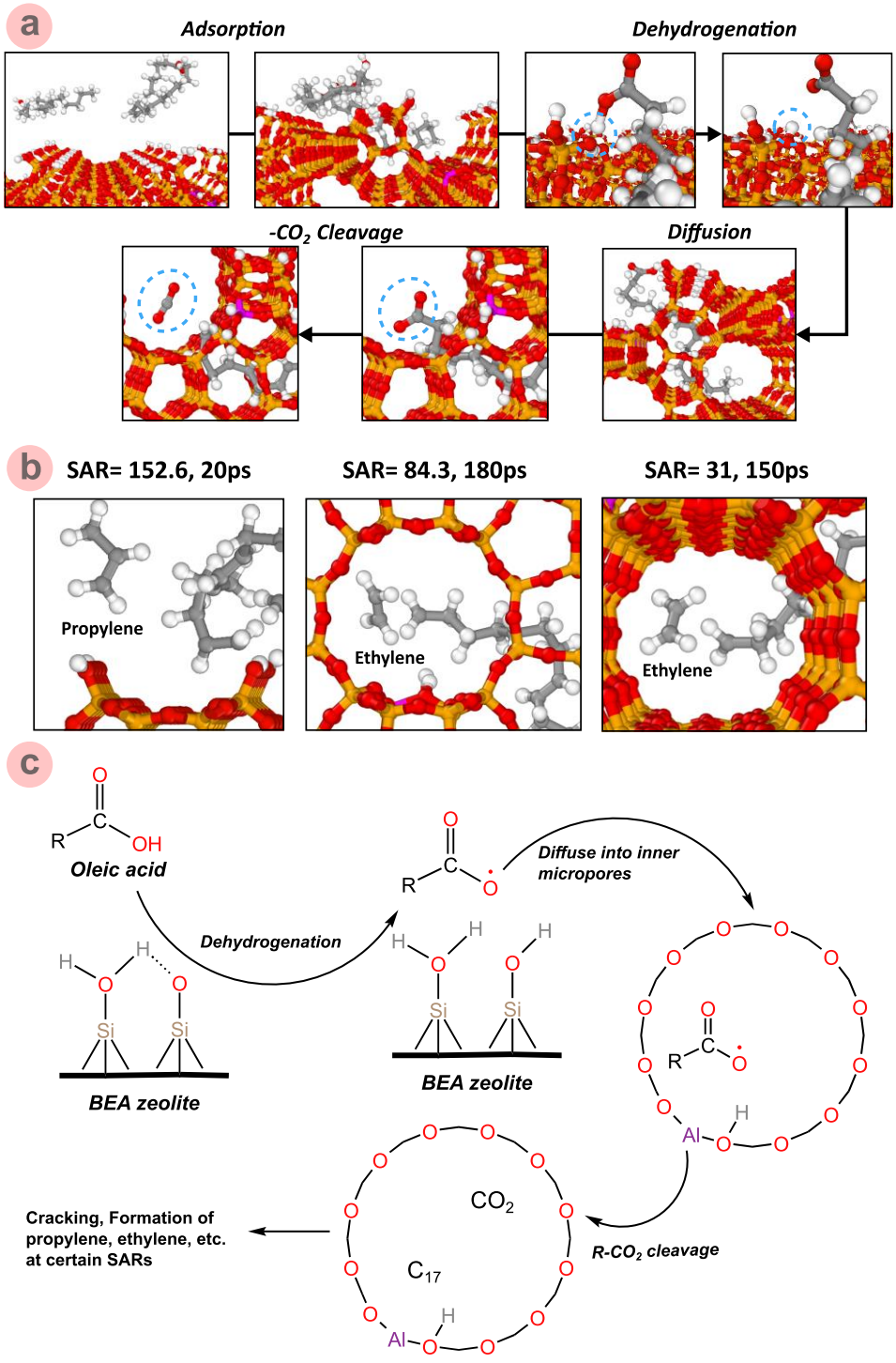

Fig. 8. (a) Sequence of oleic acid elementary reaction mechanisms starting with H-abstraction on the bridge silanol (Si-O-H-O-Si) BEA(100) structure followed by CO_2 scission in the inner BEA porous cavity. **(b)** Cracking reactions captured at certain BEA(100) SARs. Dotted blue circles are a guide for the eyes. **(c)** Schematic of the oleic acid reaction mechanism depicted by the ReaxFF simulations on BEA outer surface and inner microporous structure (*Color code: Si: orange, O: red, Al: purple, C: grey, and H: white*).

3.5. Effect of metallic dopants on the deoxygenation of the carboxyl group

Biomass upgrading benefits from the presence of both Lewis and Bronsted acid sites over porous catalysts. The metallic cations play a critical role in the selective cleavage of O-chain towards the production of hydrocarbons. Thus, we attempt to evaluate the performance of 6 selected transition metals provoked into the BEA cavity to countercharge the substitutional aluminum. Within the BEA zeolite cavity used for the DFT calculations, only a single Si atom was substituted with Al, and this alteration was counterbalanced by the incorporation of a single-atom

Please cite this article as: AlAreeqi S., Bahamon D., Alkhatib I.I.I., Polychronopoulou K., Vega L.F. Advanced computational modelling for biofuel catalyst optimization: enhancing beta zeolite acidity for oleic acid upgrading. Biofuel Research Journal 43 (2024) 2194-2210. DOI: 10.18331/BRJ2024.11.3.5.

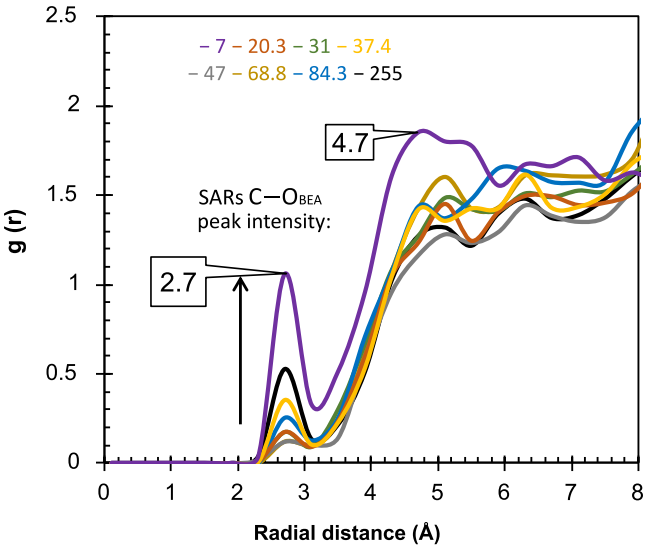

Fig. 9. Radial distribution function, $g(r)$, of O (BEA-zeolite) and C (oleic acid carbonyl) at various SARs from 7 to 255. The radial distribution function was calculated from the equilibrium configuration after 1 ns at 1200 K.

catalyst (SAC) transition metal. The SAR ratio is inconsequential in this context due to the short length scale of the DFT simulations.

Shown in **Figure 11a** is the DFT-assessed adsorption energy considering three modes of carboxylic acid (i.e., oleic acid O-fragment) adsorption on the modified BEA with SACs. O*-adsorption signals the most favorable mode for all modified SACs BEA frameworks. Notably, the rise is most marked for W-BEA. This strong Lewis acid-induced adsorption was complemented by a significant elongation in the C-O bond (1.43 Å) compared to other transition metal co-catalysts (~1.25 Å), advocating for facile deoxygenation upgrading on the W-BEA porous framework (see **Fig. 11b**). The oxygen surface separation distance O-M (i.e., M: transition metal) enables further understanding of the relative metallic oxidation/poisoning tendency, where the trend followed the order of Mo>V>W>Cu=Ni>Co, with values of 2.11>1.93>1.86>1.85 Å, respectively, placing O-W in the intermediate range.

To elucidate the single-atom catalysts coke deposition, the C* adsorption energies are depicted in **Figure 11c**. The W-doped BEA reveals the strongest chemisorption of carbon, thereby inferring excessive coking, leading to single-atom catalyst site blockage. Amidst the catalysts, Cu-BEA exhibited the minimum C* adsorption energy, indicating that while Cu-doping provides moderate E_{ads} of acetic acid, its rather lessened C* interactions imply a prolongated catalyst lifetime. This simplified descriptor (i.e., C*-adsorption energy) offers a practical property that considers the catalytic deactivation for the design of better catalyst modulations. Nonetheless, this trade-off governing the kinetics and deactivation of Lewis acid sites makes it challenging to enhance the -O cleavage reaction without compromising low C*-deposition.

3.6. Economic and environmental impact

Figure 12a compares the environmental burdens, market price, and maintenance for the transition metal catalysts. Values for Global Warming Potential (GWP) and toxicity were taken from Nuss and Eckelman (2014)'s cradle-to-gate LCA study on transition metals, while the maintenance factor was estimated based on the coke deposition evaluated in this work (**Fig. 11c**). The stronger the C*-deposition adsorption to the active site, the more prone the M-BEA catalyst to coking, hence the higher the maintenance factor allocated (see **Table S3** in the **Supplementary Material**). From **Figure 12**, several features are readily apparent. First, it can be visualized that Cu-BEA, scoring lowest in terms of coke deposition

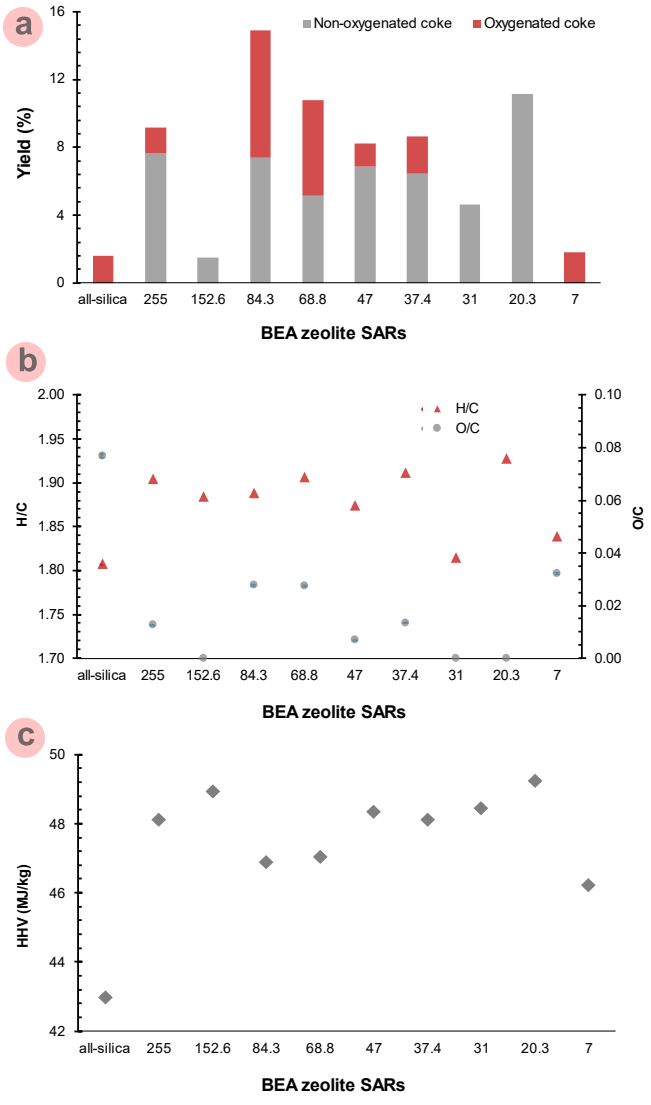

Fig. 10. Effect of BEA zeolite SARs on **(a)** the yield (%) and distribution of oxygenated and non-oxygenated coke deposition (C_{23+}), its chemical nature based on **(b)** H/C and O/C ratios, and **(c)** higher heating value (HHV). Dotted lines are a guide to the eye.

(i.e., maintenance factor), displays the lowest market price (71 USD/kg) and GWP (2.8 kg CO_2-eq/kg), yet with moderate human toxicity (0.00027 CTUh/kg). Second comes Ni, which also exhibits low environmental burdens (GWP= 6.5 kg CO_2-eq/kg, toxicity= 0.000023 CTUh/kg) and cost (85 USD/kg) but demonstrates moderate deactivation with a maintenance factor of 2. Conversely, Mo clearly displays the highest toxicity and maintenance allocation, while V reveals the highest market price and GWP.

The comparison in **Figure 12a** aids in pinpointing the cost and environmental impact associated with doping BEA for oleic acid upgrading. However, these data should be treated as a first indication of the potential implementation of the catalytic material. Further detailed techno-economic and life cycle analysis should be carried out by considering their effect on the fine-tunned BEA with SAR of 37.4 and performing the large-scale process modelling to estimate the capital and operational costs linked to their upgrading performance.

Please cite this article as: AlAreeqi S., Bahamon D., Alkhatib I.I.I., Polychronopoulou K., Vega L.F. Advanced computational modelling for biofuel catalyst optimization: enhancing beta zeolite acidity for oleic acid upgrading. Biofuel Research Journal 43 (2024) 2194-2210. DOI: 10.18331/BRJ2024.11.3.5.

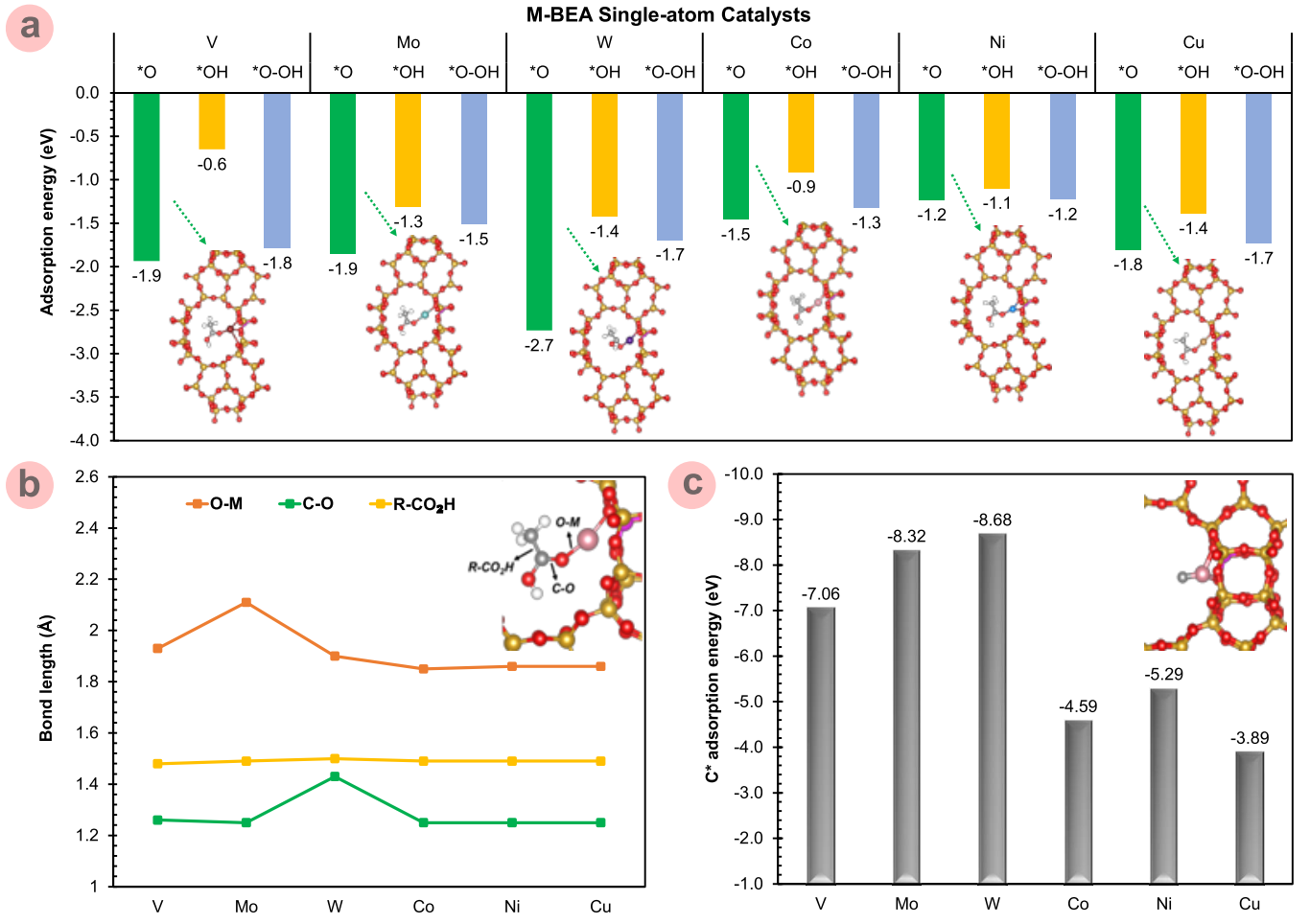

Fig. 11. DFT-calculated **(a)** adsorption energy of oleic acid oxygenated moiety (i.e., acetic acid) in the cavity of BEA zeolite modified with transition metal co-catalysts (the inserted figures represent the O*-adsorption mode for each co-catalyst system), **(b)** variations in the oxygenated moiety bond lengths resulting from acetic acid adsorption on M-promoted BEA sites, and **(c)** atomic C* adsorption energy. The inset figure in **(b)** represents the O-M, C-O, and R-CO_2H bonds, while the inset in **(c)** denotes the C* optimized adsorption conformation on M-BEA. Lines are a guide to the eyes. (*Color code: Si: orange, O: red, Al: purple, C: grey, H: white, M-dopant: pink*).

3.7. Practical implementations of the study

Figure 12b provides a variety of potential areas to advance the work presented herein and the current limitations of this study. Building on the findings presented above, the tunned BEA zeolite with SAR of 37.4, modified with Cu doping, can be investigated in terms of its impact on the reactor modelling, drop-in biofuel end-product specifications, techno-economic indicators, and life cycle emissions in future studies. Moreover, palm oil feedstock pre-processing and refining to oleic acid needs to be accounted for. The feasibility of the cultivation, physical, and chemical refining up to the biorefinery gate needs to be considered.

Apart from the exciting findings in this study, there is a need for further exploration of the applications and potential of biomass catalytic upgrading to biofuels. While the focus of this work was on BEA zeolite framework tunning, future research should prioritize implementing this computational workflow to simulate alternative biomass upgrading, including lignin, cellulose, and hemicellulose feedstocks for biofuels production. Additionally, exploring alternative catalysts, such as FAU, ZSM, or MCM-41, could unlock modified performance.

3.8. Limitations of the study

While this study investigates the complex upgrading reactions of oleic acid, several outlooks can be examined in future studies. For example, the effect of solvents, such as dodecane or water, widely applied for the HDO upgrading of fatty acids (Žula et al., 2022), can also be simulated in future studies. In addition, the effect of the hydrogen environment was not simulated in the current study, in which the focus was on the fine-tuned BEA structure and model development. While the trend and best-performing SAR are expected to remain, this is anticipated to boost the quantitative findings for drop-in fuels yields, feedstock conversion, and coke characteristics, which can be investigated in future ReaxFF simulations work. Furthermore, experimental studies on the BEA with SAR=37.4 for oleic acid upgrading can be accomplished to study the effect of reaction time and feed-to-catalyst ratio (see Fig. 12b). Such experimental tests can be performed by doping BEA with Cu, Ni, or Cu-Ni as they were shown to have great potential from the DFT calculations and the preliminary economic and environmental aspects (see Figs. 11 and 12a). Considering the doping effect, the conversion and hydrocarbon yields are expected to be significantly boosted compared to the undoped BEA catalytic materials, benefiting from both the tunned acidity and metallic active sites to drive the deoxygenation reactions.

Finally, it should be noted that the catalytic separation energy intensity is an important economic factor that needs to be examined by performing large-scale modelling to the separation stage. Moreover, this will allow a comparison of the diesel properties with conventional diesel (ASTM D975). Other than that, the results presented here are valuable to understanding the effect of acidic sites on oleic acid upgrading and provide a doorway to

Please cite this article as: AlAreeqi S., Bahamon D., Alkhatib I.I.I., Polychronopoulou K., Vega L.F. Advanced computational modelling for biofuel catalyst optimization: enhancing beta zeolite acidity for oleic acid upgrading. Biofuel Research Journal 43 (2024) 2194-2210. DOI: 10.18331/BRJ2024.11.3.5.

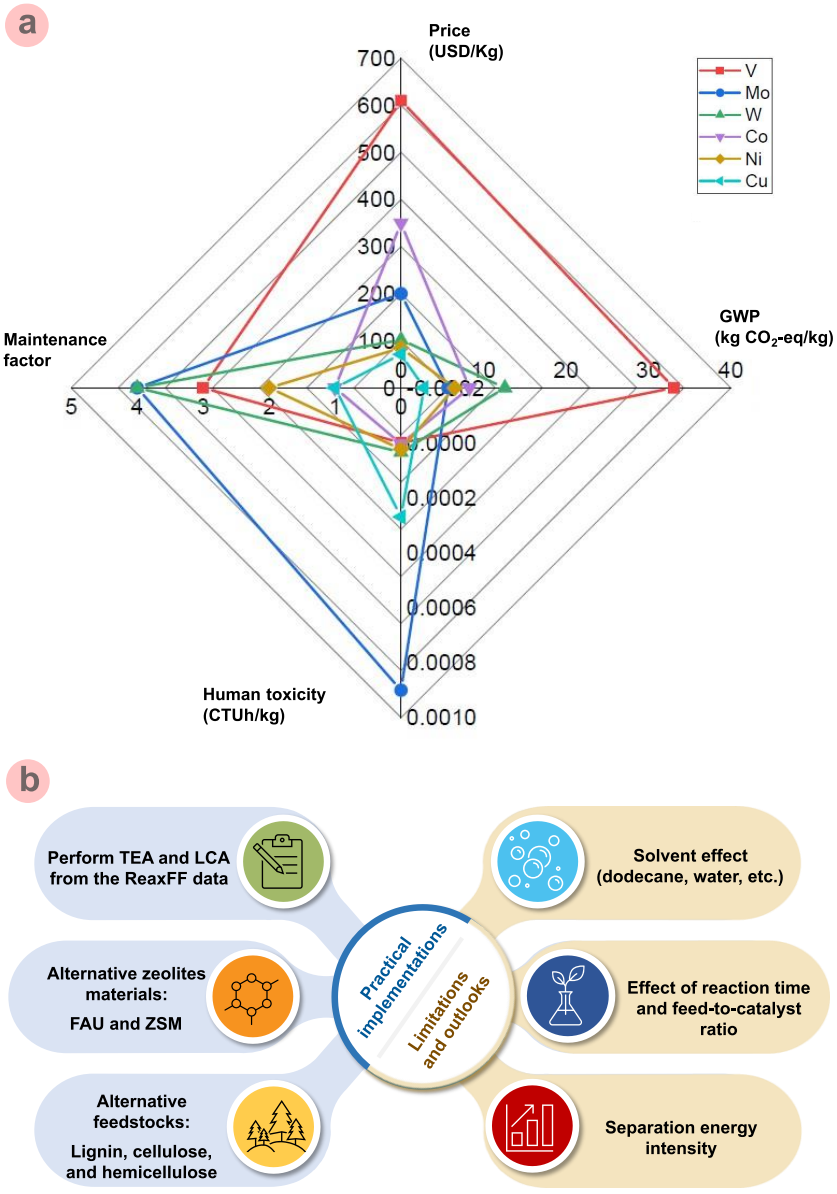

Fig. 12. (a) Radar plot of the economic and cradle-to-gate environmental aspects of transition metals studied as dopants, and **(b)** Practical implementations and limitations of this study. The maintenance factor is based on carbon adsorption energy (see **Table S3**).

implementing reactive molecular simulations as a tool for understanding and ranking biomass feedstocks catalytic upgrading.

4. Conclusions and Prospects

Catalyst deactivation caused by coke deposition is a critical performance indicator that needs to be considered in palm oil upgrading reactions on microporous catalysts/supports. A candidate pool of 9 SAR and all-silica BEA zeolite microporous structures was simulated in this work, aiming at guiding the design of zeolites with optimum SARs to improve the bio-oils conversion and selectivity towards desirable drop-in hydrocarbons while maintaining the lowest coke deposition tendency. Results revealed that the DCO_x was the predominant route favored for deoxygenation, consistent with experimental postulated mechanisms of oleic acid in "self-hydrogen supply" catalytic upgrading. A monotonic increase in DCO_x selectivity, counterpart with a steady decline in DH tendency, was found as the BEA zeolite SAR was regulated to high-silica frameworks (i.e., lowering the Al-content). Relatively high yields of diesel-range biofuel were achieved with SARs = 31, 37.4, and 68.8, while SAR = 37.4 and 47 were most effective towards gasoline biofuel. Within the diesel and gasoline range hydrocarbons, C_{17} and C_{11} exhibited the highest selectivity, respectively, while ethylene was most prevailing within the gaseous species as anticipated to form *via* the fraction of unsaturated C=C bond.

Catalytic coke formation in BEA zeolite with respect to C_{23+} quantity, oxygenated/non-oxygenated nature, and intermolecular interactions were also revealed. It was observed that the active-sites blockage involved $C_{carbonyl}$-$O_{BEA\text{-}zeolite}$ interactions, while heavy coking formation comprising ~50% oxygenated/non-oxygenated constituents was produced with SARs = 84.3 and 68.8. Interestingly, SAR = 37.4 with moderate coking characteristics and yield, exhibited the maximum oleic acid conversion dovetailed with high diesel and gasoline production.

Please cite this article as: AlAreeqi S., Bahamon D., Alkhatib I.I.I., Polychronopoulou K., Vega L.F. Advanced computational modelling for biofuel catalyst optimization: enhancing beta zeolite acidity for oleic acid upgrading. Biofuel Research Journal 43 (2024) 2194-2210. DOI: 10.18331/BRJ2024.11.3.5.

Furthermore, the incorporation of 6 transition metal catalysts into BEA zeolite unravels the effect of W-encapsulated BEA on promoting the deoxygenation reaction *via* elongating the C-O bond, yet leading to an increased susceptibility to C^*-deposition. Particularly, the Cu-BEA system exhibited minimal C^*-binding with intermediate acetic acid adsorption energy. A comparison of the 6 transition metal catalysts based on their market prices and environmental impact revealed that Cu-BEA displayed the lowest cost and GWP. Hence, from an economic point of view, the cost associated with oleic acid upgrading on BEA, even when dopped with Cu, is very appealing, which makes it a promising candidate for future studies. Furthermore, the hydrogen-free environment considered in this work minimizes risks of hazardous equipment design associated with technology scale-up.

This study served a double purpose: providing an effective strategy to tackle the atomistic coke deposition and deoxygenation mechanism of biomass-based feedstocks/aluminosilicates composites and understanding the effect tailoring the SARs in BEA zeolites towards refined drop-in biofuels production.

Acknowledgements

Financial support from Khalifa University of Science and Technology under projects RC2-2019-007, Research and Innovation Center on CO_2 and Hydrogen (RICH), and RC2-2018-024, Center for Catalysis and Separations (CeCaS), is gratefully acknowledged. Additional partial support has been provided by the Abu Dhabi Award for Research Excellence (AARE) 2019 through project AARE19-233. Computational resources from the Almesbar HPC, the research computing department at Khalifa University, and the RICH Center are also acknowledged.

References

[1] AlAreeqi, S., Bahamon, D., Polychronopoulou, K., Vega, L.F., 2022. Insights into the thermal stability and conversion of carbon-based materials by using ReaxFF reactive force field: recent advances and future directions. Carbon. 196, 840-866.

[2] Alkhoori, S., Khaleel, M., Vega, L.F., Polychronopoulou, K., 2023. Deoxygenation of vegetable oils and fatty acids: how can we steer the reaction selectivity towards diesel range hydrocarbons?. J. Ind. Eng. Chem. 127, 36-61.

[3] Asgarian, F., Hejazi, S.R., Khosroshahi, H., 2023. Investigating the impact of government policies to develop sustainable transportation and promote electric cars, considering fossil fuel subsidies elimination: a case of Norway. Appl. Energy. 347, 121434.

[4] Asikin-Mijan, N., AbdulKareem-Alsultan, G., Mastuli, M.S., Salmiaton, A., Azuwa Mohamed, M., Lee, H. V., Taufiq-Yap, Y.H., 2022. Single-step catalytic deoxygenation-cracking of tung oil to bio-jet fuel over CoW/silica-alumina catalysts. Fuel. 325, 124917.

[5] Bahamon, D., Khalil, M., Belabbes, A., Alwahedi, Y., Vega, L.F., Polychronopoulou, K., 2021. A DFT study of the adsorption energy and electronic interactions of the SO_2 molecule on a CoP hydrotreating catalyst. RSC Adv. 11(5), 2947-2957.

[6] Bai, C., Liu, L., Sun, H., 2012. Molecular dynamics simulations of methanol to olefin reactions in HZSM-5 zeolite using a ReaxFF force field. J. Phys. Chem. C. 116(12), 7029-7039.

[7] Batuer, A., Chen, D., He, X., Huang, Z., 2021. Simulation methods of cotton pyrolysis based on ReaxFF and the influence of volatile removal ratio on volatile evolution and char formation. Chem. Eng. J. 405, 126633.

[8] Bououden, W., Benguerba, Y., Darwish, A.S., Attoui, A., Lemaoui, T., Balsamo, M., Erto, A., Alnashef, I.M., 2021. Surface adsorption of Crizotinib on carbon and boron nitride nanotubes as Anti-Cancer drug Carriers: COSMO-RS and DFT molecular insights. J. Mol. Liq. 338, 116666.

[9] Chan, Y.H., Loh, S.K., Chin, B.L.F., Yiin, C.L., How, B.S., Cheah, K.W., Wong, M.K., Loy, A.C.M., Gwee, Y.L., Lo, S.L.Y., Yusup, S., Lam, S.S., 2020. Fractionation and extraction of bio-oil for production of greener fuel and value-added chemicals: recent advances and future prospects. Chem. Eng. J. 397, 125406.

[10] Chattopadhyay, A., Maiti, M.K., 2021. Lipid production by oleaginous yeasts. Adv. Appl. Microbiol. 116, 1-98.

[11] Chen, C., Volpe, R., Jiang, X., 2021. A molecular investigation on lignin thermochemical conversion and carbonaceous organics deposition induced catalyst deactivation. Appl. Energy. 302, 117557.

[12] Chizallet, C., 2020. Toward the atomic scale simulation of intricate acidic aluminosilicate catalysts. ACS Catal. 10(10), 5579-5601.

[13] Corma, A., Moliner, M., Cantín, Á., Díaz-Cabañas, M.J., Jordá, J.L., Zhang, D., Sun, J., Jansson, K., Hovmöller, S., Zou, X., 2008. Synthesis and structure of polymorph B of zeolite beta. Chem. Mater. 20(9), 3218-3223.

[14] Dabbawala, A.A., Elmutasim, O., Baker, M.A., Siakavelas, G., Anjum, D.H., Charisiou, N.D., Hinder, S.J., Munro, C.J., Gacesa, M., Goula, M.A., Polychronopoulou, K., 2023. Toward maximizing the selectivity of diesel-like hydrocarbons from oleic acid hydrodeoxygenation using Ni/Co-Al_2O_3 embedded mesoporous silica nanocomposite catalysts: an experimental and DFT approach. Appl. Surf. Sci. 640, 158294.

[15] Feng, W., Zheng, M., Bai, J., Zhang, X., Wu, C., Guo, Z., Kong, L., Bai, Z., Li, W., 2023. Dynamic structure transformation of char precursors during co-pyrolysis of coal and HDPE by using ReaxFF MD simulation and experiments. Chem. Eng. J. 472, 145100.

[16] Gea, S., Irvan, I., Wijaya, K., Nadia, A., Pulungan, A.N., Sihombing, J.L., Rahayu, R., 2022. Bio-oil hydrodeoxygenation over acid activated-zeolite with different Si/Al ratio. Biofuel Res. J. 9(2), 1630-1639.

[17] Gheewala, S.H., 2023. Life cycle assessment for sustainability assessment of biofuels and bioproducts. Biofuel Res. J. 10(1), 1810-1815.

[18] Gheewala, S.H., Jaroenkietkajorn, U., Nilsalab, P., Silalertruksa, T., Somkerd, T., Laosiripojana, N., 2022. Sustainability assessment of palm oil-based refinery systems for food, fuel, and chemicals. Biofuel Res. J. 9(4), 1750-1763.

[19] Grimme, S., Antony, J., Ehrlich, S., Krieg, H., 2010. A consistent and accurate ab *initio* parametrization of density functional dispersion correction (DFT-D) for the 94 elements H-Pu. J. Chem. Phys. 132, 154104.

[20] Grosso-Giordano, N.A., Eaton, T.R., Bo, Z., Yacob, S., Yang, C.C., Notestein, J.M., 2016. Silica support modifications to enhance Pd-catalyzed deoxygenation of stearic acid. Appl. Catal., B. 192, 93-100.

[21] Hernandez-Tamargo, C., O'Malley, A., Silverwood, I.P., De Leeuw, N.H., 2019. Molecular behaviour of phenol in zeolite Beta catalysts as a function of acid site presence: a quasielastic neutron scattering and molecular dynamics simulation study. Catal. Sci. Technol. 9(23), 6700-6713.

[22] Hoffert, M.I., Caldeira, K., Jain, A.K., Haites, E.F., Harvey, L.D.D., Potter, S.D., Schlesinger, M.E., Schneider, S.H., Watts, R.G., Wigley, T.M.L., Wuebbles, D.J., 1998. Energy implications of future stabilization of atmospheric CO_2 content. Nature. 395, 881-884.

[23] International Energy Agency, IEA. 2024. Renewables 2023, IEA, Paris.

[24] Jones, A.J., Iglesia, E., 2015. The strength of brønsted acid sites in microporous aluminosilicates. ACS Catal. 5(10), 5741-5755.

[25] Karatzos, S., van Dyk, J.S., McMillan, J.D., Saddler, J., 2017. Drop-in biofuel production via conventional (lipid/fatty acid) and advanced (biomass) routes. Part I. Biofuels, Bioprod. Biorefin. 11(2), 344-362.

[26] Kargbo, H., Harris, J.S., Phan, A.N., 2021. "Drop-in" fuel production from biomass: Critical review on techno-economic feasibility and sustainability. Renew. Sust. Energy Rev. 135, 110168.

[27] Kresse, G., Furthmüller, J., 1996. Efficient iterative schemes for ab *initio* total-energy calculations using a plane-wave basis set. Phys. Rev. B. 54, 11169.

[28] Kunamalla, A., Maity, S.K., 2023. Production of green jet fuel from furanics via hydroxyalkylation-alkylation over mesoporous MoO_3-ZrO_2 and hydrodeoxygenation over Co/γ-Al_2O_3: role of calcination temperature and MoO_3 content in MoO_3-ZrO_2. Fuel. 332, 125977.

[29] Kwon, H., Lele, A., Zhu, J., McEnally, C.S., Pfefferle, L.D., Xuan, Y., van Duin, A.C.T., 2020. ReaxFF-based molecular dynamics

Please cite this article as: AlAreeqi S., Bahamon D., Alkhatib I.I.I., Polychronopoulou K., Vega L.F. Advanced computational modelling for biofuel catalyst optimization: enhancing beta zeolite acidity for oleic acid upgrading. Biofuel Research Journal 43 (2024) 2194-2210. DOI: 10.18331/BRJ2024.11.3.5.

study of bio-derived polycyclic alkanes as potential alternative jet fuels. Fuel. 279, 118548.
[30] Lele, A., Kwon, H., Ganeshan, K., Xuan, Y., van Duin, A.C.T., 2021. ReaxFF molecular dynamics study on pyrolysis of bicyclic compounds for aviation fuel. Fuel. 297, 120724.
[31] Li, Y., Bahamon, D., Sinnokrot, M., Vega, L.F., 2022. Computational screening of transition metal-doped CdS for photocatalytic hydrogen production. npj Comput. Mater. 8, 1-9.
[32] Li, J., Gao, M., Yan, W., Yu, J., 2023a. Regulation of the Si/Al ratios and Al distributions of zeolites and their impact on properties. Chem. Sci. 14(8), 1935-1959.
[33] Li, Y., Bahamon, D., Sinnokrot, M., Vega, L.F., 2023b. Insights into the mechanisms of H2S adsorption and dissociation on CdS surfaces by DFT-D3 calculations. Int. J. Hydrogen Energy. 48(26), 9700-9712.
[34] Lian, Z., Si, C., Jan, F., Zhi, S., Li, B., 2021. Coke deposition on pt-based catalysts in propane direct dehydrogenation: kinetics, suppression, and elimination. ACS Catal. 11(15), 9279-9292.
[35] Liu, Q., Liu, S., Lv, Y., Hu, P., Huang, Y., Kong, M., Li, G., 2021. Atomic-scale insight into the pyrolysis of polycarbonate by ReaxFF-based reactive molecular dynamics simulation. Fuel. 287, 119484.
[36] Mao, Q., Feng, M., Jiang, X.Z., Ren, Y., Luo, K.H., van Duin, A.C.T., 2023. Classical and reactive molecular dynamics: principles and applications in combustion and energy systems. Prog. Energy Combust. Sci. 97, 101084.
[37] Martens, J.A., Vanbutsele, G., Jacobs, P.A., Denayer, J., Ocakoglu, R., Baron, G., Muñoz Arroyo, J.A., Thybaut, J., Marin, G.B., 2001. Evidences for pore mouth and key-lock catalysis in hydroisomerization of long n-alkanes over 10-ring tubular pore bifunctional zeolites. Catal. Today. 65(2-4), 111-116.
[38] Medeiros-Costa, I.C., Dib, E., Nesterenko, N., Dath, J.P., Gilson, J.P., Mintova, S., 2021. Silanol defect engineering and healing in zeolites: opportunities to fine-tune their properties and performances. Chem. Soc. Rev. 50(19), 11156-11179.
[39] Mortier, W.J., Ghosh, S.K., Shankar, S., 1986. Electronegativity equalization method for the calculation of atomic charges in molecules. J. Am. Chem. Soc. 108(15), 4315-4320.
[40] Nur Azreena, Lau, H.L.N., Asikin-Mijan, N., Hassan, M.A., Saiman Mohd Izham, Kennedy, E., Stockenhuber, M., Mastuli, M.S., Alharthi, F.A., Alghamdi, A.A., Taufiq-Yap, Y.H., 2021. A promoter effect on hydrodeoxygenation reactions of oleic acid by zeolite beta catalysts. J. Anal. Appl. Pyrolysis. 155, 105044.
[41] Nuss, P., Eckelman, M.J., 2014. Life cycle assessment of metals: a scientific synthesis. PLoS One. 9, 101298.
[42] Ochoa, A., Bilbao, J., Gayubo, A.G., Castaño, P., 2020. Coke formation and deactivation during catalytic reforming of biomass and waste pyrolysis products: a review. Renew. Sust. Energy Rev. 119, 109600.
[43] Ochoa, A., Valle, B., Resasco, D.E., Bilbao, J., Gayubo, A.G., Castaño, P., 2018. Temperature Programmed Oxidation Coupled with In Situ Techniques Reveal the Nature and Location of Coke Deposited on a Ni/La_2O_3-αAl_2O_3 Catalyst in the Steam Reforming of Bio-oil. ChemCatChem. 10(10), 2311-2321.
[44] Pang, Y., Zhu, X., Li, N., Wang, Z., 2023. Investigation on reaction mechanism for CO_2 gasification of softwood lignin by ReaxFF MD method. Energy. 267, 126533.
[45] Perdew, J.P., Burke, K., Ernzerhof, M., 1996. Generalized gradient approximation made simple. Phys. Rev. Lett. 77, 3865.
[46] Plimpton, S., Crozier, P., Thompson, A., 2007. LAMMPS-large-scale atomic/molecular massively parallel simulator. Sandia Natl. Lab.
[47] Polychronopoulou, K., Alkhoori, S., Albedwawi, S., Alareeqi, S., Hussien, A.G.S., Vasiliades, M.A., Efstathiou, A.M., Petallidou, K.C., Singh, N., Anjum, D.H., Vega, L.F., Baker, M.A., 2022. Decoupling the chemical and mechanical strain effect on steering the CO_2 activation over CeO_2-based oxides: an experimental and dft approach. ACS Appl. Mater. Interfaces. 14(29), 33094-33119.
[48] Qu, G., Li, S., 2023. Atomic mechanisms of long-term pyrolysis and gas production in cellulose-oil composite for transformer insulation. Appl. Energy. 350, 121695.
[49] Rambabu, K., Bharath, G., Sivarajasekar, N., Velu, S., Sudha, P.N., Wongsakulphasatch, S., Banat, F., 2023. Sustainable production of bio-jet fuel and green gasoline from date palm seed oil via hydroprocessing over tantalum phosphate. Fuel. 331, 125688.
[50] Rashidi, N.A., Mustapha, E., Theng, Y.Y., Razak, N.A.A., Bar, N.A., Baharudin, K.B., Derawi, D., 2022. Advanced biofuels from waste cooking oil via solventless and hydrogen-free catalytic deoxygenation over mesostructured Ni-Co/SBA-15, Ni-Fe/SBA-15, and Co-Fe/SBA-15 catalysts. Fuel. 313, 122695.
[51] Rey, J., Raybaud, P., Chizallet, C., 2017. Ab initio simulation of the acid sites at the external surface of zeolite beta. ChemCatChem. 9(12), 2176-2185.
[52] Shafaghat, H., Jae, J., Park, Y.K., 2021. Effect of the two-stage process comprised of ether extraction and supercritical hydrodeoxygenation on pyrolysis oil upgrading. Chem. Eng. J. 404, 126531.
[53] Shi, F., Wang, H., Chen, Y., Lu, Yanling, Hou, D., Liu, C., Lu, Yi, Lin, X., Yang, X., Zheng, Z., Zheng, Y., 2023. Green diesel-like hydrocarbon production by H_2-free catalytic deoxygenation of oleic acid via Ni/MgO-Al_2O_3 catalysts: effect of the metal loading amount. J. Environ. Chem. Eng. 11(5), 110520.
[54] Soltanian, S., Lee, C.L., Lam, S.S., 2020. A review on the role of hierarchical zeolites in the production of transportation fuels through catalytic fast pyrolysis of biomass. Biofuel Res. J. 7(3), 1217-1234.
[55] Soni, V.K., Dhara, S., Krishnapriya, R., Choudhary, G., Sharma, P.R., Sharma, R.K., 2020. Highly selective Co_3O_4/silica-alumina catalytic system for deoxygenation of triglyceride-based feedstock. Fuel. 266, 117065.
[56] Sørensen, M.R., Voter, A.F., 2000. Temperature-accelerated dynamics for simulation of infrequent events. J. Chem. Phys. 112(21), 9599-9606.
[57] Stukowski, A., 2010. Visualization and analysis of atomistic simulation data with OVITO-the Open Visualization Tool. Model. Simul. Mater. Sci. Eng. 18, 015012.
[58] Sudarsanam, P., Peeters, E., Makshina, E. V., Parvulescu, V.I., Sels, B.F., 2019. Advances in porous and nanoscale catalysts for viable biomass conversion. Chem. Soc. Rev. 48(8), 2366-2421.
[59] Taufiqurrahmi, N., Mohamed, A.R., Bhatia, S., 2010. Deactivation and coke combustion studies of nanocrystalline zeolite beta in catalytic cracking of used palm oil. Chem. Eng. J. 163(3), 413-421.
[60] van Duin, A.C.T., Dasgupta, S., Lorant, F., Goddard, W.A., 2001. ReaxFF: a reactive force field for hydrocarbons. J. Phys. Chem. A. 105(41), 9396-9409.
[61] van Duin, A.C.T., Strachan, A., Stewman, S., Zhang, Q., Xu, X., Goddard, W.A., 2003. ReaxFF SiO reactive force field for silicon and silicon oxide systems. J. Phys. Chem. A 107(19), 3803-3811.
[62] Wang, Z., Jiang, Y., Zhang, Y., Shi, J., Stampfl, C., Hunger, M., Huang, J., 2018. Identification of vicinal silanols and promotion of their formation on MCM-41 via ultrasonic assisted one-step room-temperature synthesis for beckmann rearrangement. Ind. Eng. Chem. Res. 57(16), 5550-5557.
[63] Wei, Z., Li, Y., Zhang, C., Yang, L., Chu, L., 2023. Revealing the mechanism on steam co-gasification of cellulose and polyethylene: a combined ReaxFF and DFT study. Fuel. 334, 126784.
[64] Wongnongwa, Y., Jungsuttiwong, S., Pimsuta, M., Khemthong, P., Kunaseth, M., 2020. Mechanistic and thermodynamic insights into the deoxygenation of palm oils using Ni_2P catalyst: a combined experimental and theoretical study. Chem. Eng. J. 399, 125586.
[65] World Energy Outlook 2023-Analysis-IEA.
[66] Xia, C., Cai, L., Zhang, H., Zuo, L., Shi, S.Q., Lam, S.S., 2021. A review on the modelling and validation of biomass pyrolysis with a focus on product yield and composition. Biofuel Res. J. 8(1), 1296-1315.
[67] Xiao, J., Zhang, H., Gao, X., Wang, H., Fang, G., Wang, B., Hong, C., Meng, S., 2023. Insight into pyrolysis behavior of silicone-phenolic hybrid aerogel through thermal kinetic analysis and ReaxFF MD simulations. Chem. Eng. J. 458, 141480.
[68] Yang, H., Du, X., Lei, X., Zhou, K., Tian, Y., Li, D., Hu, C., 2021. Unraveling enhanced activity and coke resistance of Pt-based catalyst in bio-aviation fuel refining. Appl. Energy. 301, 117469.

Please cite this article as: AlAreeqi S., Bahamon D., Alkhatib I.I.I., Polychronopoulou K., Vega L.F. Advanced computational modelling for biofuel catalyst optimization: enhancing beta zeolite acidity for oleic acid upgrading. Biofuel Research Journal 43 (2024) 2194-2210. DOI: 10.18331/BRJ2024.11.3.5.

[69] Yoosuk, B., Sanggam, P., Wiengket, S., Prasassarakich, P., 2019. Hydrodeoxygenation of oleic acid and palmitic acid to hydrocarbon-like biofuel over unsupported Ni-Mo and Co-Mo sulfide catalysts. Renewable Energy. 139, 1391-1399.

[70] Yusuf, B.O., Oladepo, S.A., Ganiyu, S.A., 2023. Biodiesel Production from Waste Cooking Oil via β-Zeolite-Supported Sulfated Metal Oxide Catalyst Systems. ACS Omega. 8(26), 23720-23732.

[71] Zhang, Q., Qi, Y., Hector, L.G., Çağin, T., Goddard, W.A., 2005. Atomic simulations of kinetic friction and its velocity dependence at Al/Al and α-Al_2O_3/α-Al_2O_3 interfaces. Phys. Rev. B. 72, 045406.

[72] Zheng, Y., Wang, J., Liu, C., Lu, Y., Lin, X., Li, W., Zheng, Z., 2020. Efficient and stable Ni-Cu catalysts for ex situ catalytic pyrolysis vapor upgrading of oleic acid into hydrocarbon: effect of catalyst support, process parameters and Ni-to-Cu mixed ratio. *Renew*. Energy. 154, 797-812.

[73] Zupko, R., 2019. Life cycle assessment of the production of gasoline and diesel from forest residues using integrated hydropyrolysis and hydroconversion. Int. J. Life Cycle Assess. 24, 1793-1804.

[74] Žula, M., Grilc, M., Likozar, B., 2022. Hydrocracking, hydrogenation and hydro-deoxygenation of fatty acids, esters and glycerides: mechanisms, kinetics and transport phenomena. Chem. Eng. J. 444, 136564.

Dr. Seba AlAreeqi obtained her BSc degree in Chemical Engineering from The Petroleum Institute, UAE, and her MSc and PhD in Chemical Engineering from Khalifa University of Science and Technology (2024) under the supervision of Prof Lourdes Vega. She is currently a PhD researcher at the Research and Innovation Center on CO_2 and Hydrogen (RICH) at Khalifa University. Her research focuses on the design and optimization of novel catalytic materials for sustainable fuels production using multiscale modelling techniques. Her research profile on Google Scholar can be found at the following link:
https://scholar.google.es/citations?user=FvX9SXwAAAAJ&hl=en

Dr. Daniel Bahamon obtained his BSc and MSc degrees in Chemical Engineering from the Pontifical Bolivarian University, Colombia, and his PhD in Environmental Science from the Autonomous University of Barcelona, Spain, under the supervision of Prof Lourdes Vega. He is currently a senior research scientist at the Research and Innovation Center for Graphene and 2D Materials (RIC2D) and the Research and Innovation Center on CO_2 and Hydrogen (RICH) at Khalifa University of Science and Technology. His research focuses on the design and evaluation of novel 2D materials and 3D porous materials through DFT, molecular simulations, and multiscale techniques for application in gas adsorption, catalysis, and separation processes, focused on CO_2, hydrogen, and water. His research profile on Google Scholar can be found at the following link:
https://scholar.google.pt/citations?user=8h1S_jMAAAAJ&hl=en

Prof. Kyriaki Polychronopoulou holds a PhD in Chemistry from the University of Cyprus (2005). She is currently a full professor in mechanical engineering at Khalifa University of Science and Technology, UAE, and a Visiting Professor at ETH-Zurich, Switzerland. She is also the founder and director of the Center for Catalysis and Separations (CeCaS) at Khalifa University. Her research is focused on the development of catalysts for the production of fuels with emphasis on blue hydrogen, porous adsorbents for gas separation processes, design of materials for environmental remediation (pollutants removal) as well as porous materials for H_2 storage, and CO_2 capture. Her research profile on Google Scholar can be found at the following link:
https://scholar.google.com/citations?user=gZ7QvBsAAAAJ&hl=es

Dr. Ismail I.I. Alkhatib holds a PhD in Engineering in Chemical Engineering from Khalifa University of Science and Technology under the supervision of Prof. Lourdes F. Vega. He is currently working as a postdoctoral fellow in the Research and Innovation Center on CO_2 and Hydrogen (RICH). His background is in multiscale modelling frameworks (from micro-scale thermodynamics to industry-scale technical, economic, and environmental modelling) for sustainable processes and systems focused on CO_2 capture, hydrogen production and transportation, alternative refrigeration systems, and sustainable fuels. He has a solid background in micro-scale thermodynamic modelling using advanced molecular equations of state for novel material development and their corresponding processes, including techno-economic and life cycle assessments. His research profile on Google Scholar can be found at the following link:
https://scholar.google.com/citations?user=KMt1c30AAAAJ&hl=en

Prof. Lourdes F. Vega obtained her PhD in Physics from the University of Seville, Spain, in collaboration with the Chemical Engineering Department from the University of Southern California, USA. She has developed her career between academia and industry. Full Professor in Chemical Engineering at Khalifa University in the UAE, she is also the Director and Founder of the Research and Innovation Center on CO_2 and Hydrogen (RICH) and Theme lead for energy and hydrogen in the Research and Innovation Center on Graphene and 2D materials (RIC2D). Her research revolves around moving fundamental science to industrial applications by combining multiscale modelling with experiments focused on CO_2 capture and utilization, hydrogen, sustainable fuels, water treatment, and cooling systems. Her research profile on Google Scholar can be found at the following link:
https://scholar.google.pt/citations?user=RUesAz0AAAAJ&hl=en

Please cite this article as: AlAreeqi S., Bahamon D., Alkhatib I.I.I., Polychronopoulou K., Vega L.F. Advanced computational modelling for biofuel catalyst optimization: enhancing beta zeolite acidity for oleic acid upgrading. Biofuel Research Journal 43 (2024) 2194-2210. DOI: 10.18331/BRJ2024.11.3.5.

Supplementary Material

Table S1.
The number of gaseous molecules used to obtain HDO, DCOX, and DH selectivity. Results are averaged over the last 100ps of the ReaxFF simulations.

SARs	Number of Molecules			
	CO_2	CO	H_2O	H_2
all-silica	12	1	7	35.5
255	37	1	6	67.5
152.6	37	0	7	71
84.3	37	1	3	75.5
68.8	36	0	2	80
47	36	0	3	82.5
37.4	35	0	5	82.5
31	35	1	5	92
20.3	33	0	4	101.5
7	13	1	13	126

Table S2.
Bond lengths of acetic acid resulting from its adsorption on M-promoted BEA sites. M stands for transition metal co-catalysts: V, Mo, W, Co, Ni, and Cu.

	V	Mo	W	Co	Ni	Cu
O-M (Å)	1.93	2.11	1.90	1.85	1.86	1.86
C-O (Å)	1.26	1.25	1.43	1.25	1.25	1.25
C-CO_2H (Å)	1.48	1.49	1.50	1.49	1.49	1.49

Table S3.
Allocated maintenance factor based on C^*-adsorption on M-promoted BEA zeolite.

C^* adsorption energy (eV)	-3.5—5.0	-5.0—-6.5	-6.5 – -8.0	-8.0 – -9.5
Maintenance factor	1	2	3	4

Please cite this article as: AlAreeqi S., Bahamon D., Alkhatib I.I.I., Polychronopoulou K., Vega L.F. Advanced computational modelling for biofuel catalyst optimization: enhancing beta zeolite acidity for oleic acid upgrading. Biofuel Research Journal 43 (2024) 2194-2210. DOI: 10.18331/BRJ2024.11.3.5.

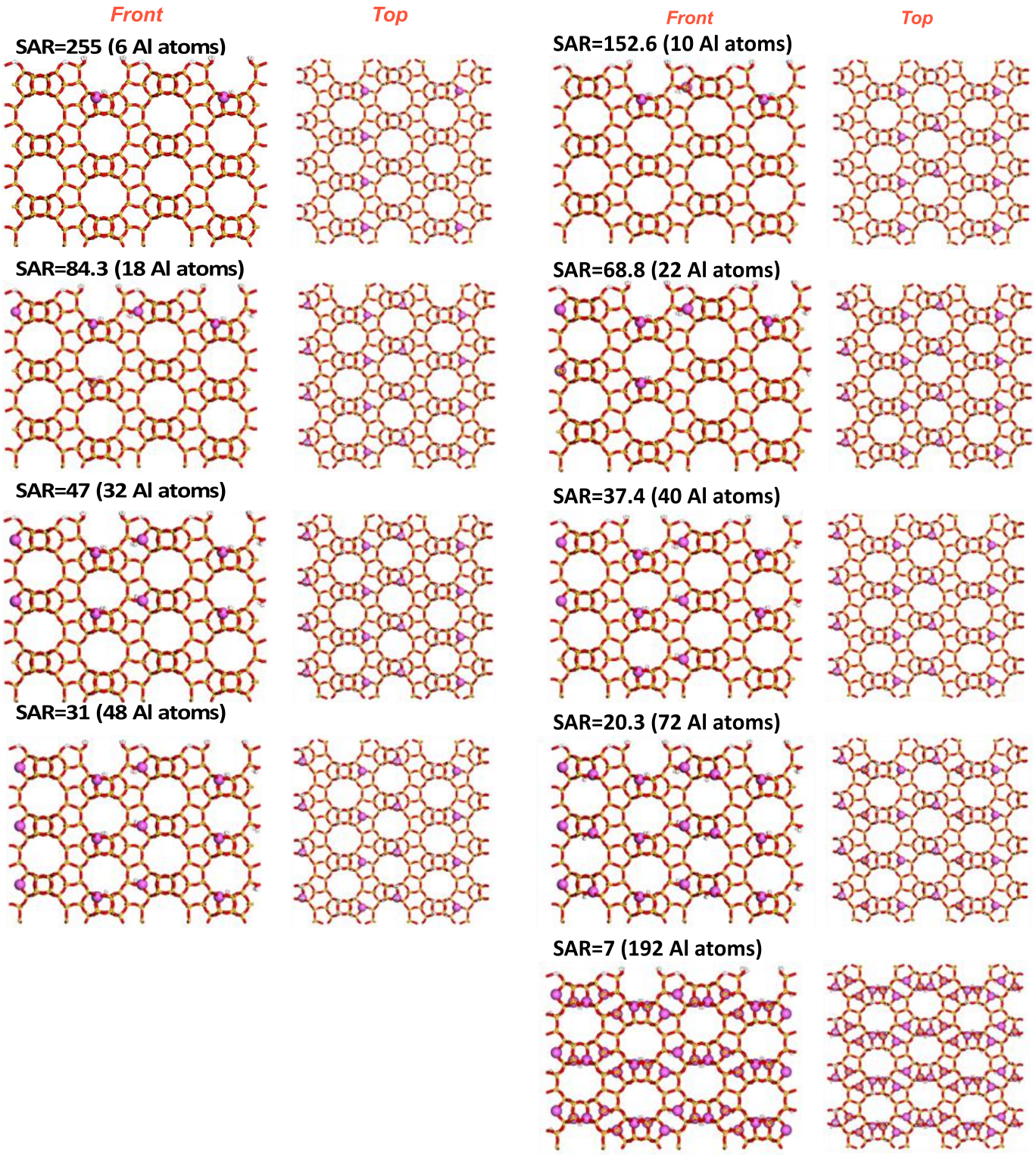

Fig. S1. Front (1st and 3rd columns) and Top (2nd and 4th columns) views of BEA zeolite model development with tuned SARs from 255 to 7.

Please cite this article as: AlAreeqi S., Bahamon D., Alkhatib I.I.I., Polychronopoulou K., Vega L.F. Advanced computational modelling for biofuel catalyst optimization: enhancing beta zeolite acidity for oleic acid upgrading. Biofuel Research Journal 43 (2024) 2194-2210. DOI: 10.18331/BRJ2024.11.3.5.

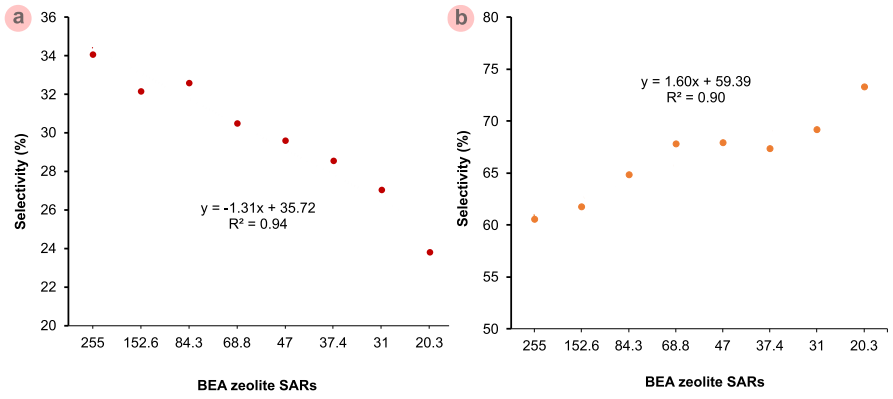

Fig. S2. Linear derived correlation of **(a)** decarboxylation/decarbonylation (DCO_x) and **(b)** dehydrogenation (DH) selectivity (%) of oleic acid catalytic reactions on H-BEA(100) with respect to varying silica-to-alumina ratio (SARs) from 20.3 to 255.

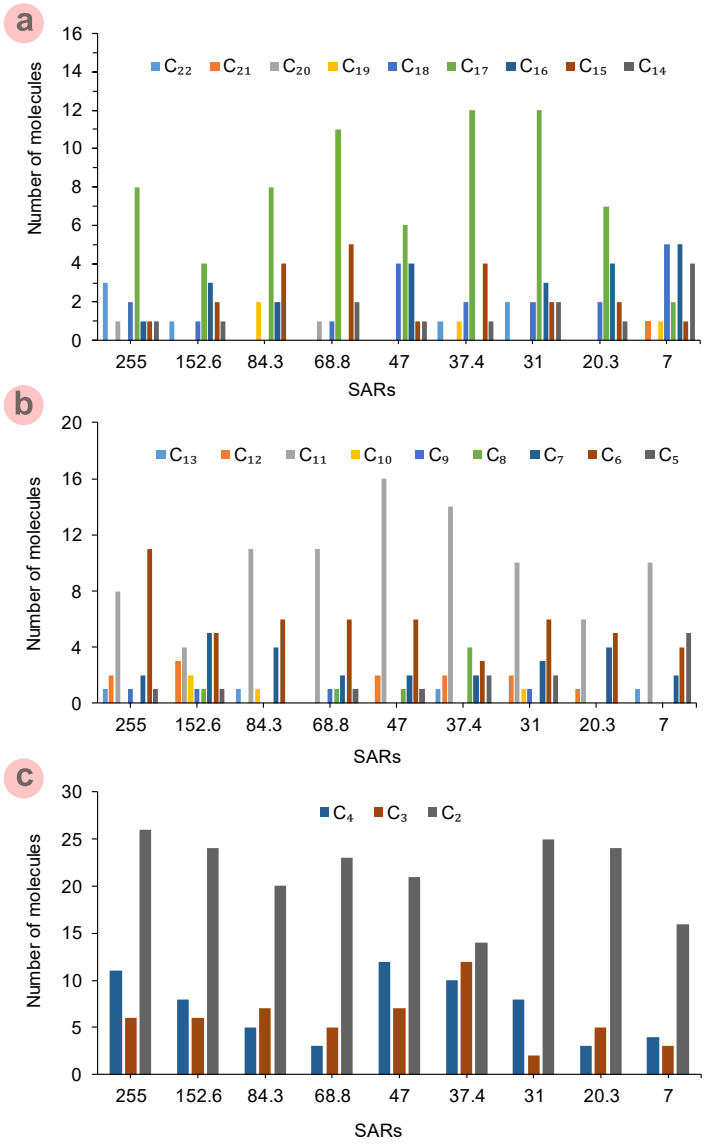

Fig. S3. Effect of SAR on the number of **(a)** C2-C4, **(b)** C5-C13, and **(c)** C14-C22 species formed from oleic acid upgrading on BEA-zeolite.

Please cite this article as: AlAreeqi S., Bahamon D., Alkhatib I.I.I., Polychronopoulou K., Vega L.F. Advanced computational modelling for biofuel catalyst optimization: enhancing beta zeolite acidity for oleic acid upgrading. Biofuel Research Journal 43 (2024) 2194-2210. DOI: 10.18331/BRJ2024.11.3.5.

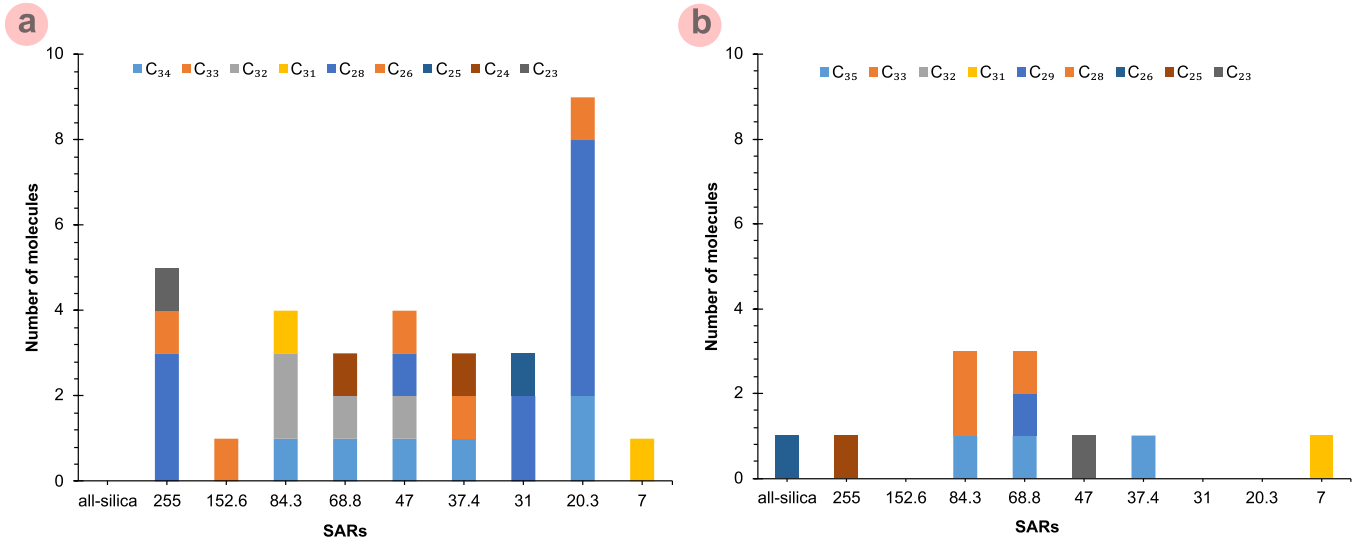

Fig. S4. The number of derived **(a)** non-oxygenated and **(b)** oxygenated coke (C_{23+}) molecules at the various BEA(100) silica to alumina ratios (SARs).

The higher heating value (HHV) of the coke fragments has been evaluated using Dulong's formula (**Eq. S1**) (Channiwala and Parikh, 2002; Ochoa et al., 2020):

$$HHV(MH.kg^{-1}) = \left[338.8.W_C + 1442.8.\left(W_H - \frac{W_O}{8}\right) + 94.2W_S\right].10^{-3} \quad \text{Eq. S1}$$

where W_C, W_H, W_O, and W_S denote the mass fractions of carbon, hydrogen, oxygen, and sulfur present in the coke sample, respectively.

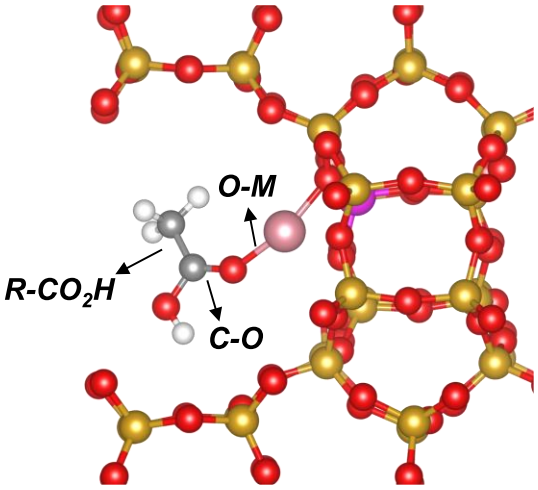

Fig. S5. Representation of reported bond lengths in **Table S2** (*Color code: Si: orange, O: red, Al: purple, C: grey, H: white, and M-dopant: pink*).

References

[1] Channiwala, S.A., Parikh, P.P., 2002. A unified correlation for estimating HHV of solid, liquid and gaseous fuels. Fuel. 81(8), 1051-1063.
[2] Ochoa, A., Bilbao, J., Gayubo, A.G., Castaño, P., 2020. Coke formation and deactivation during catalytic reforming of biomass and waste pyrolysis products: a review. Renew. Sust. Energy Rev. 119, 109600.

Please cite this article as: AlAreeqi S., Bahamon D., Alkhatib I.I.I., Polychronopoulou K., Vega L.F. Advanced computational modelling for biofuel catalyst optimization: enhancing beta zeolite acidity for oleic acid upgrading. Biofuel Research Journal 43 (2024) 2194-2210. DOI: 10.18331/BRJ2024.11.3.5.